UNIVERSITY OF BELGRADE

FACULTY OF MECHANICAL ENGINEERING

ABDELNASER ABSALAM MOKHTAR ELAYEB

ANALYSIS OF RASTER ANGLE INFLUENCE ON TENSILE MECHANICAL PROPERTIES OF ADDITIVELY MANUFACTURED COMPOSITE PLATES MADE FROM PET-G POLYMER REINFORCED WITH SHORT CARBON FIBERS

DOCTORAL DISSERTATION

BELGRADE, 2024

УНИВЕРЗИТЕТ У БЕОГРАДУ
МАШИНСКИ ФАКУЛТЕТ

АБДЕЛНАСЕР АБДУСАЛАМ МОКХТАР ЕЛАЈЕБ

АНАЛИЗА УТИЦАЈА УГЛА ДЕПОНОВАЊА НА ЗАТЕЗНЕ МЕХАНИЧКЕ КАРАКТЕРИСТИКЕ АДИТИВНО ПРОИЗВЕДЕНИХ КОМПОЗИТНИХ ПЛОЧА НАПРАВЉЕНИХ ОД ПЕТ-Г ПОЛИМЕРА ОЈАЧАНОГ КРАТКИМ УГЉЕНИЧНИМ ВЛАКНИМА

ДОКТОРСКА ДИСЕРТАЦИЈА

БЕОГРАД, 2024

SUPERVISOR:

Dr. Igor Balać, full time professor

University of Belgrade, Faculty of Mechanical Engineering

.....

BOARD OF COMMISSION:

Dr. ……..

…….

.....

Dr. ……..

…….

.....

Dr. ……..

……

.....

DEDICATION

To my esteemed mother, father, beloved wife, cherished children, supportive brothers and sisters, and invaluable educators at every level of my education, I am honored to dedicate this thesis to you. Your unwavering support, guidance, and inspiration have played a pivotal role in my academic achievements, and for that, I express my everlasting gratitude

ACKNOWLEDGMENT

Firstly, I would like to thank ***God Almighty*** and thank Him for His grace, mercy, and generosity. Without his guidance, I would not have achieved the success I have today.

Secondly, I would also like to express my sincere appreciation to my supervisor, **Prof. Dr. Igor Balać**, who played an essential role in helping me overcome various challenges with his vast knowledge and experience. His valuable comments contributed greatly to the completion of this thesis. I would like to thank **Prof. Dr. Alexander Grbović** for his continuous and constant support, which helped me during my study period to the best of my ability. I am also grateful to the staff at the Faculty of Mechanical Engineering and my friends, whose help and support were invaluable during the research process. Finally, I would like to thank my father for his continuous support and encouragement during my studies, despite his suffering, and my mother, whose prayers motivated me to succeed. I would also like to thank my wife, who has been a pillar of strength and patience throughout this journey. Her inexhaustible support and prayers have been instrumental in completing this dissertation. I extend my thanks to my family members, my children, as well as to my brothers and sisters in Libya, for their support, patience and prayers during my studies. ☺

ABSTRACT

In additive manufacturing (AM), raster angle is recognized as one of the key printing parameters which strongly influences the strength and stiffness of the final part. In this thesis the effect of raster angle on tensile properties and anisotropic behaviour of additively manufactured composite plates made from PET-G polymer reinforced with short carbon fibers are studied. The functional relations between the corresponding raster angle and obtained values of tensile strength and the tensile elastic constants which define the anisotropic behaviour of studied material (modulus of elasticity - E_x, Poisson's coefficient - ν_{xy} and coefficient of mutual influence of the second kind - $n_{xy,x}$) are established. Aforementioned functional relations are compared with theoretical results based on the Classical Lamination Theory (CLT). The ultimate tensile strength average value of 52.2 MPa obtained for specimens printed with the raster angle of 0° is noticeably higher than the average value obtained for specimens printed with the raster angle of 90° - 25.4 MPa. Correspondingly, the maximum average value of 4752 MPa for modulus of elasticity is obtained for specimens printed with the raster angle of 0°, substantially higher compared to the value of 1569 MPa obtained for specimens printed with the raster angle of 90°. The fracture surfaces of the tested specimens are inspected under SEM - images of the specimens printed with the 0° raster angle revealed dominant alignment of short carbon fibers with the printing direction applied, but also moderate to high level of inhomogeneity and voids. While analysing the SEM images, considerable volume fraction of captured air is noticed, together with porosity presence in polymer phase, which are recognised as probable major contributors in relatively low improvement of tensile strength (from what was expected) obtained for carbon reinforced samples made with the 0° printing direction, when compared to neat polymer samples. Similarly, voids together with weak bonding between two adjacent rasters undoubtedly served as influential factors for poor tensile properties of carbon reinforced samples made with the raster angle of 90°. Comparison of the estimated values calculated by the CLT expression for modulus of elasticity - E_x, with experimentally obtained values, showed almost perfect matching (mismatching was less than 10% for the whole raster angle range). In case of Poisson's coefficient - ν_{xy} and coefficient of mutual influence of the second kind - $n_{xy,x}$ mismatching was higher than 10% for the whole raster angle range. Thus, comparison of the estimated values calculated by the CLT expression for Poisson's coefficient - ν_{xy}, with experimentally obtained values, showed significant mismatching particularly in 45°- 75° raster angle range. Similarly, comparison of the estimated values calculated by the CLT expression for coefficient of mutual influence of the second kind - $n_{xy,x}$ with experimentally obtained values, showed significant mismatching particularly in 15°- 60° raster angle range.

***Keywords**: composite plates; additive manufacturing; raster angle; tensile mechanical properties; short carbon fibers*

САЖЕТАК

У адитивној производњи угао депоновања материјала је препознат као један од кључних параметара процеса добијања (штампе) делова који у великој мери утиче на чврстоћу и крутост завршног дела. У овој тези се проучава утицај угла депоновања материјала на затезна механичка својства и анизотропно понашање адитивно произведених композитних плоча од ПЕТ-Г полимера ојачаног кратким угљеничним влакнима. Функционалне релације између одговарајућег угла депоновања и добијених вредности затезне чврстоће и затезних константи еластичности које дефинишу анизотропно понашање проучаваног материјала (модул еластичности - E_x, Поасонов коефицијент - ν_{xy} и коефицијент узајамног утицаја друге врсте - $n_{xy,x}$). Поменуте функционалне зависности су упоређене са теоријским резултатима заснованим на Класичној теорији ламинације (*CLT*). Просечна вредност затезне чврстоће од 52,2 MPa добијена за узорке штампане са углом депоновања од 0° је приметно виша од просечне вредности добијене за узорке штампане са углом депоновања од 90° - 25,4 MPa. У складу са тим, максимална просечна вредност модула еластичности од 4752 MPa добијена је за узорке штампане са углом депоновања од 0°, што је знатно више у поређењу са вредношћу од 1569 MPa добијеном за узорке штампане са углом депоновања од 90°. Преломне површине испитаних узорака су анализиране помоћу СЕМ снимака – слике узорака штампаних са углом депоновања од 0° откривају доминантно поравнање кратких угљеничних влакана са примењеним смером штампе (углом депоновања), али и умерен до висок ниво нехомогености и присуства „заробљеног“ ваздуха. Анализом СЕМ снимака примећује се значајан запремински удео „заробљеног“ ваздуха, заједно са порозношћу у полимерној фази, који су препознати као вероватни главни фактори који доприносе релативно ниском побољшању затезне чврстоће (од онога што се очекивало) добијеном за узорке ојачане угљеничним влакнима направљеним са углом депоновања од 0°, у поређењу са узорцима од „чистог“ полимера. Слично томе, нехомогености заједно са слабом везом између две суседне линије штампе несумњиво су послужиле као утицајни фактори за ниска затезна својства угљеником ојачаних узорака направљених са углом депоновања од 90°. Поређење процењених вредности израчунатих *CLT* изразом за модул еластичности - E_x са експериментално добијеним вредностима, показало је скоро савршено поклапање (неусклађеност је мања од 10% за цео опсег углова депоновања). У случају Поасоновог коефицијента - ν_{xy} и коефицијента узајамног утицаја друге врсте - $n_{xy,x}$, неусклађеност је била већа од 10% за цео распон углова депоновања. Дакле, поређење процењених вредности израчунатих *CLT* изразом за Поасонов коефицијент - ν_{xy} са експериментално добијеним вредностима, показало је значајно неслагање посебно у опсегу угла депоновања од 45° до 75°. Слично, поређење процењених вредности израчунатих *CLT* изразом за коефицијент међусобног утицаја друге врсте - $n_{xy,x}$ са експериментално добијеним вредностима показало је значајно неслагање посебно у опсегу угла депоновања од 15° до 60°.

Кључне речи: *композитне плоче; адитивна производња; угао депоновања; затезна механичка својства; кратка угљенична влакна*

Contents

1 Introduction, literature survey and objectives of the research

1.1 Introduction

1.1.1 Background

When establishing research into composite materials, the term *composite* is first introduced and therefore should be explained in its broadest sense. The term *composite* refers to a system consisting of two or more ingredients with different material properties, designed to obtain enhanced final product's properties compared to those characterising the individual constituents. Typically, mechanical properties of the constituents largely differ. One of them is usually discontinuous, stiffer and stronger and is called the *reinforcement*, whereas the less stiff and weaker one is continuous and is called the *matrix* [1].

Fibers are the most common reinforcing and load-bearing element of the composites, while the matrix has the function of transferring the load to the fibers in addition to holding the fibers together. Therefore, the matrix gives the composite a geometric shape.

Carbon fibers used as reinforcements in composite materials, are without a doubt the most widespread today, especially in the heavily loaded parts of structures where high stiffness and strength together with low mass are required. Usual properties of carbon fibers are the following: diameter of 5-10 μm, density of 1.75-1.9 g/cm^3, strength of 2.5-5.5 GPa, modulus of elasticity of 240-400 GPa and breaking strain at 1-2 % [2]. As such, they represent an excellent choice for the reinforcement, most often in combination with an epoxy matrix, for high-performance structural composites, which are used in the aerospace and automotive industries.

The basic functions of the matrix in the composite material are:
- transferring the load to the reinforcements,
- separating the reinforcements from each other,
- forming an external shape of the composite structure,
- potentially protecting from environmental influences.

That being the case, properties of the matrix often determine the properties of the whole composite, as well as its application limitations in terms of external influential agents (moisture, temperature, etc.). Also, properties of the matrix are important for determining the longitudinal tensile strength, transverse strength and interlayer shear strength of the composite [3].

When talking about polymers used as matrices in composites, they can be divided into two groups: thermosets and thermoplastics. When heated, thermosets (thermostable polymers) create irreversible chemical bonds between polymer chains that are strongly cross-linked. When reheated, they do not change their state, but remain rigid. This points to a big problem in their application, which is increasingly important nowadays – it is not possible to recycle them by softening the matrix, but only to grind them mechanically, which results in small granules that contain both fibers and matrix. Unlike them, thermoplastics have the property that they harden when cooled, but soften when reheated, so they can be shaped again. This enables the repair of parts made from these composites, as well as their partial recycling.

Moreover, thermoplastics are used in processes including extrusion, thermoforming and injection moulding. Common thermoplastics include polyethylene (PE), polycarbonate (PC), polyvinylchloride (PVC), polypropylene (PP), polystyrene (PS) and polyethylene terephthalate (PET), the last with added glycol (PET-G) being the choice for further examining throughout this thesis as a matrix material for obtaining the studied composite plate specimens.

The characteristic temperature called the *glass transition temperature - (GTT)* is a very important property of the matrix and defines the transition between the soft rubbery state of a polymeric matrix and its more stiff, or glassy, state [4]. This temperature defines the final properties of the matrix in terms of the usability of the composite at elevated temperatures. Namely, when used above the glass transition temperature, the properties of the matrix are significantly degraded. It should be noted that moisture in the composite can significantly lower the glass transition temperature.

The technology of making the composite significantly affects its final properties, because it must ensure a good bond between the fiber and the matrix, as well as a minimal fraction of porosity or micro-cracks in the composite. Additive manufacturing (AM), more commonly known as 3D printing, is the process of additively building up a part one layer at a time (see Figure 1). There are a range of 3D printing technologies with each having their own benefits and limitations and each being able to print parts from different materials [6]. Extrusion based AM, known as Fused Deposition Modelling (FDM) or Fused Filament Fabrication (FFF), has become a widespread AM technique. As a result, the development and production of polymer-based parts via AM is a continuously emerging research trend [7].

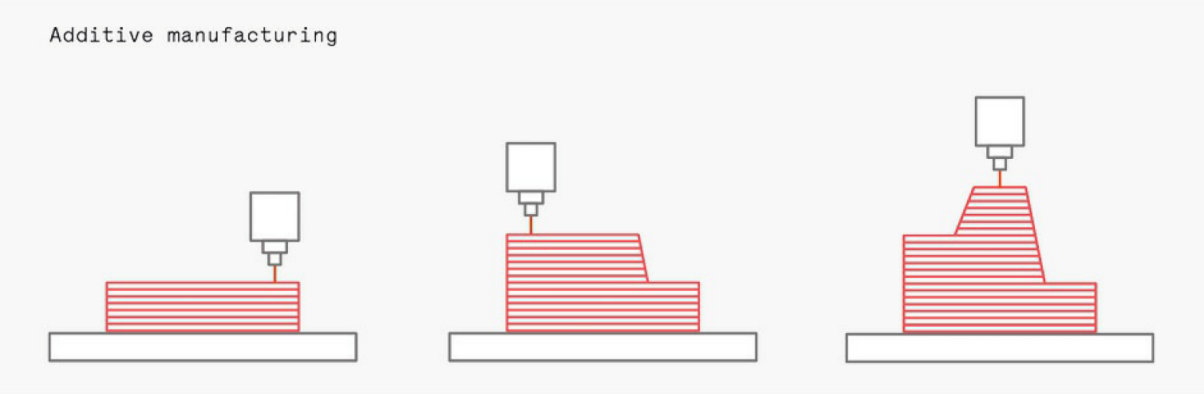

Figure 1.1 *A schematic of how additive manufacturing technologies produce parts [6]*

Carbon Fiber Reinforced Polymers (CFRP) in additive manufacturing gained much engineering attention in recent decade because of the potential for superior structural performance compared to base polymeric feedstock materials. In general, an anisotropic and heterogeneous character of the obtained composite material provides the composite with many degrees of freedom for optimum configuration of the material system [1]. Therefore, carbon reinforcements put in filaments used for additive manufacturing receive researchers' attention as well – demands for material characterization, design and optimisation. That being the case, despite AM offers considerable freedom in design and production of 3D printed parts, anisotropy and inhomogeneity of final product still remain uncertain [8, 9], so there is current need for contribution in analysing and predicting the mechanical properties of such parts made from reinforced polymeric materials (actually composite materials).

1.1.2 Classification of composite materials based on the geometry of reinforcement

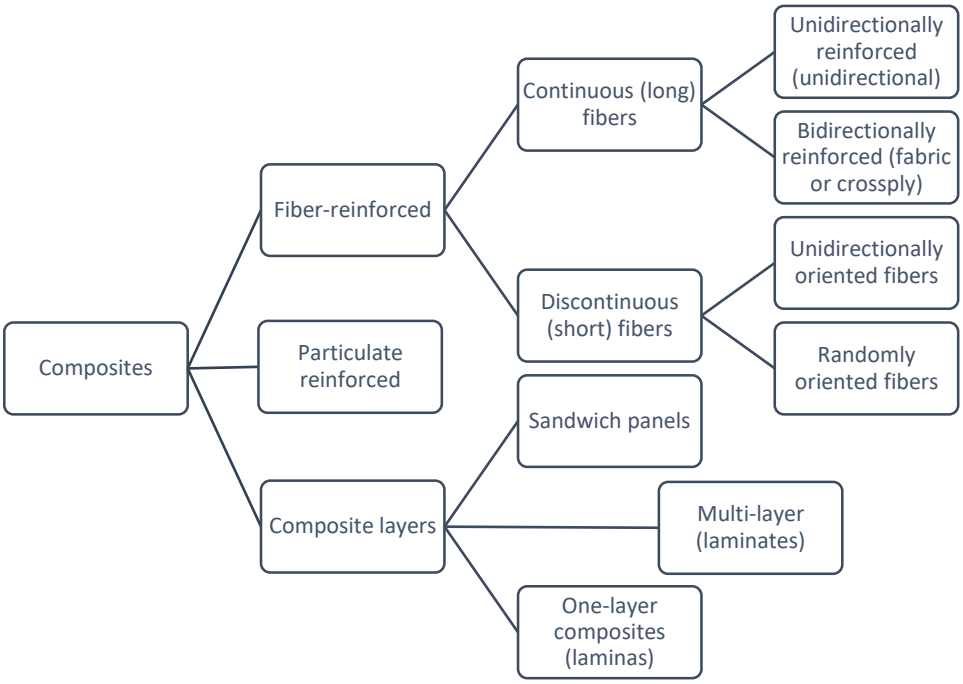

Figure 1.2 *Composites classification [5]*

The term *laminated composites* is used to define layers of material usually reinforced with long continuous fibers. These layers can contain fibers laying within differently oriented directions and are called *laminas*. Laminas that are interconnected (glued) into one unbreakable unit form a multi-layer composite, so-called *laminate*.

Since polymers have limited mechanical properties, aiming to make FDM suitable for producing functional load-bearing parts, Short Carbon Fibers (SCF) have been introduced into polymeric feedstock materials as reinforcements [10]. Although continuous fiber reinforced composites offer higher mechanical performance, their processing through FDM is not commonplace due to printing complexity [11]. On the other hand, short fiber reinforced polymers (SFRPs) are used more often due to availability of feedstock materials and low-cost fabrication, but with moderately improved mechanical properties [12, 13, 14]. Composites reinforced with fibers generally differ in their properties from conventional engineering materials. Conventional engineering materials (like steel) are almost always considered to be isotropic and homogeneous. In the case of an isotropic material, the physical and mechanical characteristics are the same in all directions, and a homogeneous material is a material that has a uniform composition or the same composition in every point or particle of the body. In this thesis, polymeric thin plates reinforced with milled SCF of around 200 μm in length, suitable for FDM processing on desktop 3D printers, will be considered.

1.1.3 Fused Deposition Modelling (FDM) and process parameters

Aforementioned fused deposition modelling as an additive manufacturing (3D printing) technique implies material extrusion through a heated nozzle, melting it in the process and depositing on a build platform in a predetermined path, where the material cools and solidifies to form a solid part [6]. In extrusion-based additive manufacturing final printed part has

material properties which differ from those of the filament material used for its fabrication. This difference arises from the FDM process parameters, mainly the following ones [15, 16, 17]:

- build orientation (flat, on-edge, upright – see Figure 1.3),
- printing direction (raster angle),
- layer thickness,
- infill density,
- infill print speed,
- extrusion width,
- nozzle temperature and
- printing bed temperature.

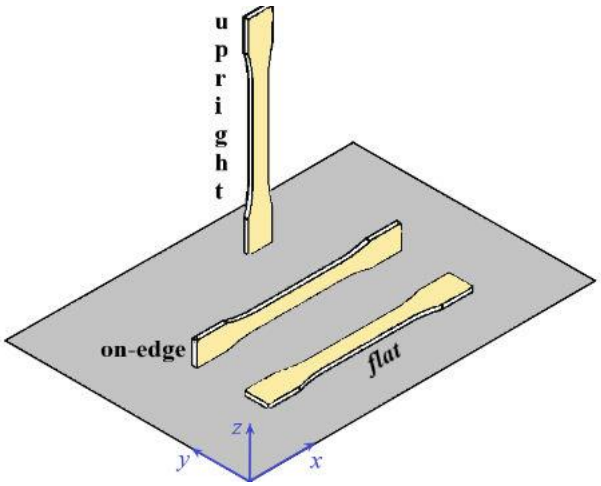

Figure 1.3 *Build orientation in FDM*

The layer-by-layer FDM nature leads to final parts that are generally characterised by discrete mechanical properties in different directions. The FDM process parameters altogether and their different combinations can actually intensify the anisotropic nature of AM parts. Therefore, it is of great importance to correctly understand how the process parameters influence performance of the final part and optimise them to match the intended application.

The printing direction commonly referred to as the *raster angle* appear to be one of the main influential parameters, especially for those parts printed with flat build orientation [8, 18]. Therefore, the raster angle has been selected for further observation throughout the thesis as determination of its influence on tensile properties of specific AM parts may be a valuable research activity. Additionally, the presence of porosity within the extruded material, especially the reinforced one, could also be research appealing, since various kinds of potential polymer-reinforcement mixing originated inhomogeneities may substantially degrade final part's mechanical properties such as strength and stiffness [19, 20]. This is particularly important when material is used for producing parts as structural members intended for carrying load.

1.2 Literature survey

Apart from six textbooks on Mechanics of Composite Materials (Refs. [1-5, 34]) and one handbook on 3D Printing Technologies (Ref. [6]), number of scientific papers (Refs. [7-33]) covering various issues related to the thesis topic have served as the basis for the candidate's research and guided further work on the thesis.

The review papers [21, 22] contain a comprehensive overview of additive manufacturing techniques, as well as a review of the base materials used in additive manufacturing and their mechanical properties. Since polymer-based structures reinforced with fibers provide improved properties of functional parts in use, such as lower density compared to conventional materials, but also increased mechanical performances compared to base materials ("neat" polymers), the review paper [21] additionally emphasizes the importance and potential of developing such parts through additive manufacturing technologies and their application as structural elements. Noticeable progress in newly developed polymer and composite materials and the recentness of their production by additive manufacturing are also addressed. In the review paper [23], a detailed description of the previous experimental approaches to these materials' characterization and attempts for constitutive models definition was given, aiming to summarize the applicability and limitations of these approaches. Additionally, paper [22] lists the common ASTM and ISO standards used by different research groups for testing the mechanical properties of parts obtained by additive manufacturing.

As one of the conclusions based on the technological state-of-the-art review, the paper [9] highlights the possibility of improving the characteristics of new materials by using carbon fibers as reinforcements of polymeric base materials exploited in additive manufacturing. The analyses of final mechanical characteristics carried out on additively manufactured polymer parts reinforced with short carbon fibers are discussed in papers [10, 11, 18, 24, 25, 26]. In the paper [24] polypropylene (PP) is considered as the base material, while papers [11, 26] encompass ABS polymer and paper [10] additionally observes PLA and PET-G polymers. Papers [18, 27, 28] examine the relevance of the mechanics of conventional composite laminates for characterizing the mechanical behaviour of additively manufactured parts, i.e. possibilities and limitations of the application of classical lamination theory.

The occurrence of anisotropy in additively manufactured polymeric parts is analysed in the paper [16], with a detailed review of previous research aimed at understanding the nature of this phenomenon as well as the main factors and parameters that affect the intensity of this phenomenon. When depositing melted filament in FDM as the most common technique of additive manufacturing, inhomogeneities in various forms of "trapped" air between the deposited material lines as well as between adjacent layers appear, resulting in the weakening of mechanical properties. The pores between the deposited lines that follow the applied raster angle, together with the causes of the anisotropic behaviour occurrence and the consequent effects on the mechanical characteristics are investigated in the paper [29] for ABS polymer reinforced with short carbon fibers.

The influence of different FDM parameters is evaluated in papers [15, 17, 30, 31] dedicated to the study of production parameters' effects on the tensile strength and stiffness of the obtained parts. The paper [30] emphasized the influence of raster angle on the mechanical properties and thermal conductivity of additively manufactured composites of PP polymer reinforced with

short carbon fibers. The building orientation throughout the deposition process, layer thickness and printing speed as influential parameters are observed in the paper [15], nozzle temperature and again printing speed in the paper [17], while paper [31] examines nozzle diameter and the gap between the two deposited lines (rasters) as influential parameters in the FDM process.

In the available literature, a lack of analysis comprehending the raster angle influence on the mechanical properties of composites additively manufactured from PET-G polymer reinforced with different percentages of short carbon fibers is noticed, as well as a lack of the raster angle impact assessment on the anisotropy occurrence and its intensity in this type of material. Also, there is a lack of model proposals that would establish the functional relation between the elastic constants and strength properties on one hand and the raster angle on the other, concerning thin-plate parts obtained by additive manufacturing using the here considered composite material (PET-G polymer reinforced with short carbon fibers).

1.3 Objectives of the research

Within this doctoral thesis, the following objectives of the research are acknowledged:

- Analysis of the raster angle influence on the tensile mechanical properties (stiffness and strength) of additively manufactured plates made of PET-G polymer reinforced with SCF suitable for FDM;

- Establishment of a functional relation between the measured values of tensile strength and stiffness and the corresponding raster angle;

- Determination of the tensile elastic constants for different raster angles that define the anisotropic behaviour of the observed type of material composition, primarily the coefficient of mutual influence of the second kind which represents the coupling between the occurrence of sliding in the plane of the sample and the effect of normal stress during uniaxial tension;

- Establishment of a functional relation between the values of elastic constants and the value of raster angle, as well as comparison of these functional relations with the results given by the Classical Lamination Theory (CLT).

It is expected that after the realization of the research objectives, the thesis will contribute to the definition of future constitutive model that will enable the application of numerical structural analysis on thin plate-like parts made from observed material composition and produced by additive manufacturing. Accordingly, it is also expected that the dissertation will contribute to a better understanding and further enhancements in possible applications of this type of composite materials for quick and efficient production of parts intended for moderate loadings.

- Initial hypotheses of the thesis

The initial hypotheses based on the literature review are the following:

1. The use of composite parts made of PET-G polymer reinforced with short carbon fibers is possible for load-bearing members that are intended for moderate intensity loadings.

2. It is possible to establish a linear relationship between the stress tensor and the strain tensor for this type of material in the elastic deformation region.

3. It is possible to determine all the elastic constants that define the anisotropic behaviour of this type of composite material by conducting appropriate experimental testing.

4. The change of elastic constants with the value of raster angle can be presented by applying the principles of the Classical Lamination Theory (CLT).

- Research methods

The following research methods and approaches are proposed:

1. Analysis of the existing approaches as well as previous engineering knowledge base of the subject thesis area. This involves a review of the available literature relevant to the topic of the doctoral thesis.

2. Statement of the considered problem (description method).

3. Combined analytical-experimental methods for determining all elastic constants that define the anisotropic behaviour of the observed type of composite material.

4. Experimental methods for the purpose of contemplating and verifying the previously mentioned calculations (comparison method).

1.4 The structure of the thesis

The thesis is structured into six main Chapters, as summarised within the following:

Chapter 1 comprises basic information on the composite material and its constituents in general (matrix and reinforcement), classification of composite materials based on the geometry of reinforcement and introductory notes about the Additive Manufacturing, particularly its extrusion based technique called Fused Deposition Modelling. The material which will be further analysed throughout the thesis is defined in this Chapter, together with the manufacturing technique which will be utilised, as well as objectives of the research, initial hypotheses and research methods. Literature survey for the previously defined area of research is given briefly at the end of this Chapter.

In **Chapter 2**, the fundamentals of elasticity of anisotropic body are outlined in short, referring to general state of stress and strain, leading to their relations represented through matrix layout of generalised Hook's law. A simplified form of the general Hook's law for the orthotropic body is then given in this Chapter, as a step towards lamina-related equations known from Classical Lamination Theory, to later check if applicable to the results containing mechanical performances of thin-plate samples examined in the thesis. Fundamentals of mechanics of composite materials are continued with thin plates reinforced with continuous fibers. Hooke's law for an orthotropic plate for the case of plane stress is presented, together with the remaining non-zero coefficients of the compliance matrix. Here it was essential to provide relations between elastic constants and compliance matrix coefficients known from Classical Lamination Theory (CLT) for composite plates reinforced with continuous fibers. This gives basic understanding critical for the subsequent study aimed to inspect if experimental results

obtained for additively manufactured thin-plate samples made derived from PET-G polymer reinforced with short carbon fibers would fit those CLT curves.

Chapter 3 is referenced to PET-G polymer based plates reinforced with short carbon fibers. The Short Carbon Fibers (SCF) used as reinforcements of filaments intended for extrusion based additive manufacturing (FDM) are observed more closely. The focus is on the percent fraction of SCF and their orientation within filament. On top of that, raster angle as influential parameter of FDM process is addressed as key factor to investigate further throughout the thesis, i.e. its influence on tensile mechanical properties of the surveyed thin-plate samples.

In **Chapter 4** experimental procedure and obtained results are demonstrated. Samples used for testing are specified along with FDM process parameters used for their fabrication. Tensile testing results are presented, preceded by explanation of the experimental setup used, including the universal testing machine and Digital Image Correlation (DIC) apparatus. Finally, evaluated elastic constants are delivered together with assessed strength properties of the samples tested.

Chapter 5 establishes functional relations between the obtained values for tensile elastic constants and the applied raster angle, as well as between calculated strength properties and corresponding raster angle. This Chapter is the key one since it combines already known analytical methods and experimental measurements producing relevant data for the purpose of contemplating and verifying the anisotropic behaviour of the observed type of composite material.

Chapter 6 brings conclusions of the thesis and provides recommendations for future research which would advance the findings established in the thesis.

2 Mechanics of fiber reinforced composite plates

2.1 Generalised Hook's law for an anisotropic body

Formulating equations which describe material's behaviour in terms of deformation under the influence of external load, i.e. defining the equations that relate stress to strain for all load-cases, can be extremely complex. If these equations can be formulated, then they are called constitutive equations of the material. The set of all these equations for a material is called the constitutive model of material behaviour. The best way to define a constitutive model, ie. connections between stress and strain are appropriate experiments.

It is clear that it is almost impossible to formulate a single equation or a set of equations that will fully describe the material's behaviour in all possible conditions. However, for a load below a certain limit, almost all structural materials that carry (transmit) loads, deform elastically, so for that range of deformations and loads, a set of equations is formulated that relate stress and strain. However, when the load exceeds a certain limit, the material begins to deform inelastically, so additional deformation parameters are necessary to calculate the stress in that range. These problems are dealt with in detail by special scientific fields such as Theory of plasticity and Mechanics of fracture.

2.1.1 General state of stress

If three stress vectors are known for a certain point for three mutually perpendicular intersecting planes passing through that point, we can say that we know the stress state in it. As it is necessary to know 3 data (components of the vector) to define each vector, it is clear that 9 data are necessary to know the stress at a certain point, namely stress components (Figure 2.1). As a result, the stress at a point represents a higher form of abstraction than a vector and in continuum mechanics represents a tensor of the second order.

A tensor can be described as a mathematical representation of a physical quantity in defined coordinate system. If one piece of data is sufficient for the representation of a physical quantity in some coordinate system, such physical quantity is a zero-order tensor - a scalar quantity (e.g. mass, temperature), if three pieces of data are sufficient, then it is a first-order tensor - a vector quantity (e.g. force, speed). In the case when nine data are required, then physical quantity represents a second-order tensor (e.g. stress, strain), etc. In continuum mechanics, operations with tensors are performed using the so-called tensor calculus. The state of stress at a point of a stressed body, in the general three-dimensional case, for orthogonal coordinate system defined by the axes x, y, z (forming the planes x–y, y–z, x–z), can be described by stress tensor which have nine stress components as shown in Figure 2.1. Usually, stress tensor is presented in following matrix notation:

$$\{\sigma\} = \begin{bmatrix} \sigma_x & \tau_{xy} & \tau_{xz} \\ \tau_{yx} & \sigma_y & \tau_{yz} \\ \tau_{zx} & \tau_{zy} & \sigma_z \end{bmatrix} \tag{2.1}$$

where σ_i is component of normal stress, while τ_{ij} is component of shear stress. The subscript of normal stress refers to the axis direction in which the stress component acts. The first

subscript of shear stress component refers to the direction of the outward normal to the face on which the stress component acts, while the second subscript refers to the direction in which the stress component itself acts. All of stress components shown in Figure 2.1 have positive sign.

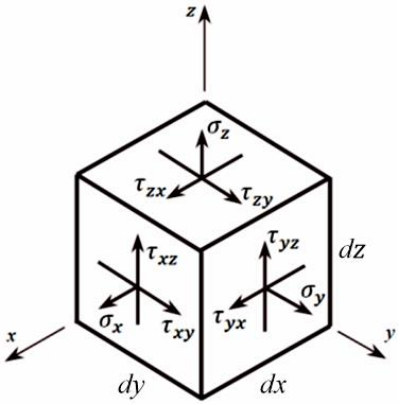

Figure 2.1 *Three-dimensional stress state*

2.1.2 General state of strain

In the general case of exposing the body to external loads, the body is deformed. When the body is deformed, there are translational and/or angular movements (rotation) of points inside the stressed body. The state of strain at a point is completely determined if the components of strain are known for 3 mutually perpendicular directions, that is, for 3 mutually perpendicular planes to which these directions are normal. Then we say that the strain tensor at that point is known. The strain tensor, as the second-order tensor, is usually written as a 3x3 matrix of the form:

$$\{\varepsilon\} = \begin{bmatrix} \varepsilon_x & \varepsilon_{xy} & \varepsilon_{xz} \\ \varepsilon_{yx} & \varepsilon_y & \varepsilon_{yz} \\ \varepsilon_{zx} & \varepsilon_{zy} & \varepsilon_z \end{bmatrix} = \begin{bmatrix} \varepsilon_x & \frac{1}{2}\gamma_{xy} & \frac{1}{2}\gamma_{xz} \\ \frac{1}{2}\gamma_{yx} & \varepsilon_y & \frac{1}{2}\gamma_{yz} \\ \frac{1}{2}\gamma_{zx} & \frac{1}{2}\gamma_{zy} & \varepsilon_z \end{bmatrix} \tag{2.2}$$

where ε_x, ε_y and ε_z are normal strains which describe the extension or contraction per unit length along the x, y and z direction, respectively, while γ_{ij} is shear strain (describe the distortional deformations associated with lines that were originally parallel to the i and j axes). It is important to make a difference between the component of "tensor" strain - ε_{ij} and the component of "engineering" shear strain - γ_{ij}. Engineering shear strain γ_{ij} describes the total distortional change in the angle between lines that were originally parallel to the x_i and x_j axes, but the tensor shear strain ε_{ij} describes the amount of rotation of either of the lines.

2.1.3 Generalised Hook's law

As it is well known from any book related to Theory of elasticity, both stress and strain are symmetric tensors (i.e., $\tau_{ij} = \tau_{ji}$ and $\gamma_{ij} = \gamma_{ji}$) so that there are only six independent stress components and six independent strain components. Having that in mind, in general case, in some point of stressed anisotropic body made from the linear elastic material, components of stress are related to components of strain through the following relationship, usually called Generalised Hook's law:

$$\begin{bmatrix} \sigma_x \\ \sigma_y \\ \sigma_z \\ \tau_{yz} \\ \tau_{xz} \\ \tau_{xy} \end{bmatrix} = \begin{bmatrix} C_{11} & \cdots & C_{16} \\ \vdots & \ddots & \vdots \\ C_{61} & \cdots & C_{66} \end{bmatrix} \begin{bmatrix} \varepsilon_x \\ \varepsilon_y \\ \varepsilon_z \\ \gamma_{yz} \\ \gamma_{xz} \\ \gamma_{xy} \end{bmatrix} \tag{2.3}$$

or in compact form:

$$[\sigma] = [C][\varepsilon]$$

In the above equations, matrix $[C]$ is called stiffness matrix while coefficients C_{ij} are called stiffness matrix coefficients. Total number of stiffness matrix coefficients is 36.

It is clear that by inverting the above equation, components of strain can be expressed via stresses in matrix form:

$$\begin{bmatrix} \varepsilon_x \\ \varepsilon_y \\ \varepsilon_z \\ \gamma_{yz} \\ \gamma_{xz} \\ \gamma_{xy} \end{bmatrix} = \begin{bmatrix} S_{11} & \cdots & S_{16} \\ \vdots & \ddots & \vdots \\ S_{61} & \cdots & S_{66} \end{bmatrix} \begin{bmatrix} \sigma_x \\ \sigma_y \\ \sigma_z \\ \tau_{yz} \\ \tau_{xz} \\ \tau_{xy} \end{bmatrix} \tag{2.4}$$

or in compact form:

$$[\varepsilon] = [S][\sigma]$$

In the above equations, matrix $[S]$ is called compliance matrix while coefficients S_{ij} are called compliance matrix coefficients or elastic compliances. It is obvious that stiffness matrix and compliance matrix are related as inverted matrices:

$$[C] = [S]^{-1} \tag{2.5}$$

Total number of compliance matrix coefficients is 36 (same as the number of stiffness matrix coefficients). As shown in any mechanics of materials book, due to the existence of the strain energy density, the stiffness and compliance matrices are also symmetric. Due to this fact, only 21 of the 36 elastic compliances are independent. Similarly, the stiffness matrix has also only 21 independent stiffness matrix coefficients.

Sometimes, *stiffness* and *compliance constants* are referred to as *elastic constants*. Once these constants are found for a particular point, the stress and strain relationship can be developed (at that point). Note that these constants can vary from point to point if the material is

nonhomogeneous. Even if the anisotropic material is homogeneous (or assumed to be), one needs to find these 21 elastic constants experimentally.

In case of anisotropic material stiffness and compliance matrix coefficients are dependent on the coordinate system – in other words, they change with rotation of coordinate system.

2.1.4 Stress-strain relationship for orthotropic body

Consider the case when the body has three mutually orthogonal planes of material property symmetry as shown in Figure 2.2 where planes 1–2, 2–3 and 3–1 are planes of material symmetry. In that case the 1,2 and 3 coordinate axes are referred to as the *principal material coordinates*. The body which has three planes of elastic symmetry is-called **orthotropic** body - orthogonally isotropic material. It can be easily shown that the equations of the general Hooke's law can be simplified when the body possesses planes of material symmetry.

The Hooke's law for an orthotropic material, with planes 1–2, 2–3 and 3–1, as planes of material symmetry, for three dimensional stress state (Figure 2.3) can be written in the following form:

$$\begin{bmatrix}\sigma_1\\ \sigma_2\\ \sigma_3\\ \tau_{23}\\ \tau_{13}\\ \tau_{12}\end{bmatrix} = \begin{bmatrix}C_{11} & C_{12} & C_{13} & 0 & 0 & 0\\ C_{12} & C_{22} & C_{23} & 0 & 0 & 0\\ C_{13} & C_{23} & C_{33} & 0 & 0 & 0\\ 0 & 0 & 0 & C_{44} & 0 & 0\\ 0 & 0 & 0 & 0 & C_{55} & 0\\ 0 & 0 & 0 & 0 & 0 & C_{66}\end{bmatrix}\begin{bmatrix}\varepsilon_1\\ \varepsilon_2\\ \varepsilon_3\\ \gamma_{23}\\ \gamma_{13}\\ \gamma_{12}\end{bmatrix} \tag{2.6}$$

The above equation represents the constitutive relations between stresses and strains in linear – elastic orthotropic materials – Hooke's law for an orthotropic body. An example of such material is the unidirectional carbon fiber reinforced composite lamina shown in Figure 2.4.

By inverting the stiffness matrix, the strain-stress relation is obtained in the inverse form:

$$\begin{bmatrix}\varepsilon_1\\ \varepsilon_2\\ \varepsilon_3\\ \gamma_{23}\\ \gamma_{13}\\ \gamma_{12}\end{bmatrix} = \begin{bmatrix}S_{11} & S_{12} & S_{13} & 0 & 0 & 0\\ S_{12} & S_{22} & S_{23} & 0 & 0 & 0\\ S_{13} & S_{23} & S_{33} & 0 & 0 & 0\\ 0 & 0 & 0 & S_{44} & 0 & 0\\ 0 & 0 & 0 & 0 & S_{55} & 0\\ 0 & 0 & 0 & 0 & 0 & S_{66}\end{bmatrix}\begin{bmatrix}\sigma_1\\ \sigma_2\\ \sigma_3\\ \tau_{23}\\ \tau_{13}\\ \tau_{12}\end{bmatrix} \tag{2.7}$$

Here, engineering constants need to be defined. The engineering constants are costants that engineers use to describe the mechanical behaviour of a material. Thus, in *Mechanics of materials*, *engineering constants* (sometimes known as *elastic constants*) are known as: *Modulus of elasticity* (E), *Poisson's ratio* (ν) and *Shear modulus* (G). Usually, these constants are evaluated experimentally by conducting simple tests such as tension or pure shear tests. Therefore, it is logical, as well as practical, to express stiffness and compliance coefficients in Equations (2.6) and (2.7) in terms of appropriate engineering constants.

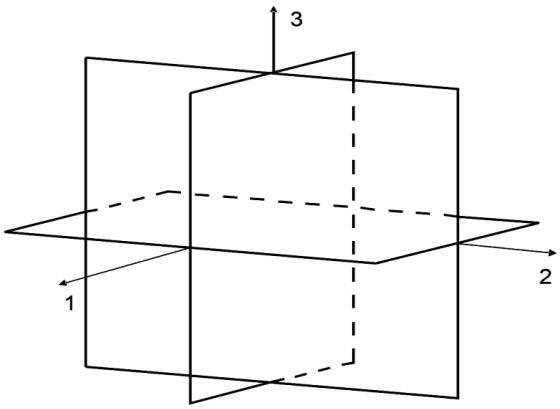

Figure 2.2 *An orthotropic material - the material which has 3 mutually orthogonal planes of material symmetry*

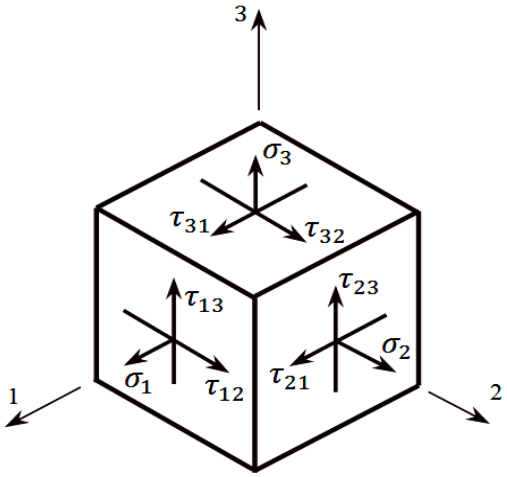

Figure 2.3 *A three-dimensional stress state, at a point in 1–2–3 orthogonal coordinate system*

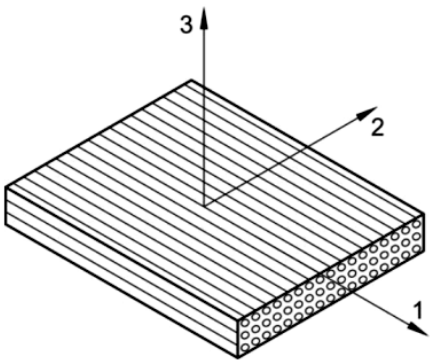

Figure 2.4 *The unidirectional composite lamina*

It is the fact that compliance matrix coefficients appearing in equation (2.7) are much easier to determine in terms of appropriate engineering constants. For the purpose of defining compliance matrix coefficients in terms of appropriate engineering constants a series of tests presented in Figure 2.5 should be performed.

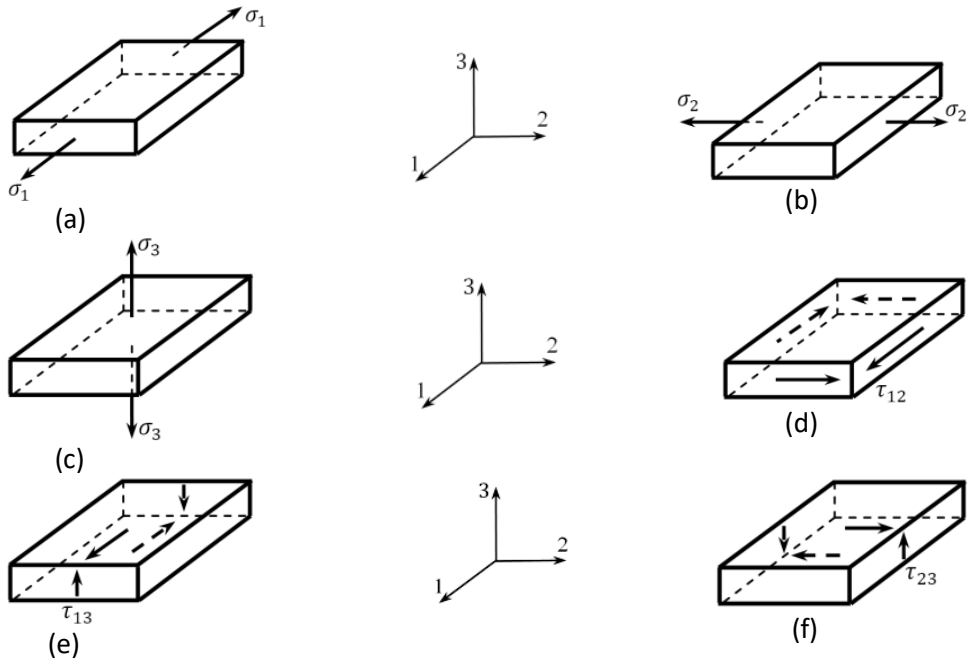

Figure 2.5 *Experiments for determining the compliance matrix coefficients*

Thus, after conducted experiments, presented in Figure 2.5, the following engineering constants of orthotropic body should be known: values of modulus of elasticity for the principal material directions (E_1, E_2, E_3), values of shear moduli in the pricipal material planes (G_{12}, G_{13}, G_{23}) as well as values of Poisson coefficients in principal material planes $(\nu_{12}, \nu_{13}, \nu_{23}, \nu_{21}, \nu_{31}, \nu_{32})$. Consequently, it can be easily shown that the compliance matrix for the orthotropic material, equation (2.7), may be presented in the following form:

$$[S] = \begin{bmatrix} \frac{1}{E_1} & -\frac{\nu_{12}}{E_1} & -\frac{\nu_{13}}{E_1} & 0 & 0 & 0 \\ -\frac{\nu_{21}}{E_2} & \frac{1}{E_2} & -\frac{\nu_{23}}{E_2} & 0 & 0 & 0 \\ -\frac{\nu_{31}}{E_3} & -\frac{\nu_{32}}{E_3} & \frac{1}{E_3} & 0 & 0 & 0 \\ 0 & 0 & 0 & \frac{1}{G_{23}} & 0 & 0 \\ 0 & 0 & 0 & 0 & \frac{1}{G_{13}} & 0 \\ 0 & 0 & 0 & 0 & 0 & \frac{1}{G_{12}} \end{bmatrix} \tag{2.8}$$

Now, Hooke's law for an orthotropic material, for principal material axes 1, 2 and 3, can be written in the following form, where the strain components are expressed in terms of stresses:

$$\begin{bmatrix} \varepsilon_1 \\ \varepsilon_2 \\ \varepsilon_3 \\ \gamma_{23} \\ \gamma_{13} \\ \gamma_{12} \end{bmatrix} = \begin{bmatrix} \frac{1}{E_1} & -\frac{\nu_{12}}{E_1} & -\frac{\nu_{13}}{E_1} & 0 & 0 & 0 \\ -\frac{\nu_{21}}{E_2} & \frac{1}{E_2} & -\frac{\nu_{23}}{E_2} & 0 & 0 & 0 \\ -\frac{\nu_{31}}{E_3} & -\frac{\nu_{32}}{E_3} & \frac{1}{E_3} & 0 & 0 & 0 \\ 0 & 0 & 0 & \frac{1}{G_{23}} & 0 & 0 \\ 0 & 0 & 0 & 0 & \frac{1}{G_{13}} & 0 \\ 0 & 0 & 0 & 0 & 0 & \frac{1}{G_{12}} \end{bmatrix} \begin{bmatrix} \sigma_1 \\ \sigma_2 \\ \sigma_3 \\ \tau_{23} \\ \tau_{13} \\ \tau_{12} \end{bmatrix} \tag{2.9}$$

Important to remember that the values of coefficients of the stiffness matrix as well as the compliance matrix in anisotropic material depend on the reference coordinate system, in other words, they change if the coordinate system is changed and therefore: $C_{ij}^{xy} \neq C_{ij}{}^{12}$ ($S_{ij}^{xy} \neq S_{ij}{}^{12}$)

2.2 Stress-Strain Relationships for thin plate - Plane Stress State

A thin plate is a prismatic member having a small thickness. A plate shown in Figure 2.6 is primarily loaded in its own plane x–y (there are no out-of-plane loads). If the upper and lower surfaces of the plate are free from external loads, then $\sigma_z = \tau_{zx} = \tau_{zy} = 0$.

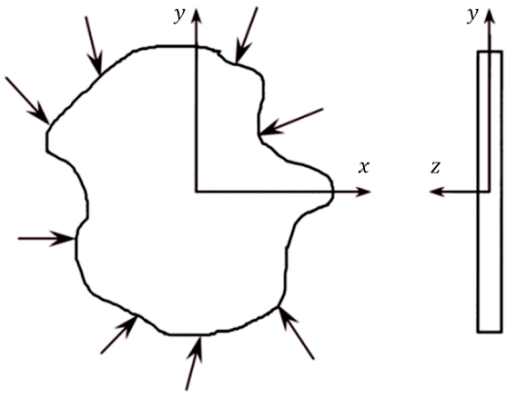

Figure 2.6 *A thin plate loaded in its own plane x–y*

If the plate is assumed to be thin, these three stresses within the plate are assumed to vary little from the magnitude of stresses at the top and the bottom surfaces. Thus, stresses σ_z , τ_{zx} and τ_{zy} can be assumed to be zero within the plate also, while the non-zero stresses σ_x, σ_y and τ_{xy} have uniform distribution through plate thickness (see Figure 2.7).

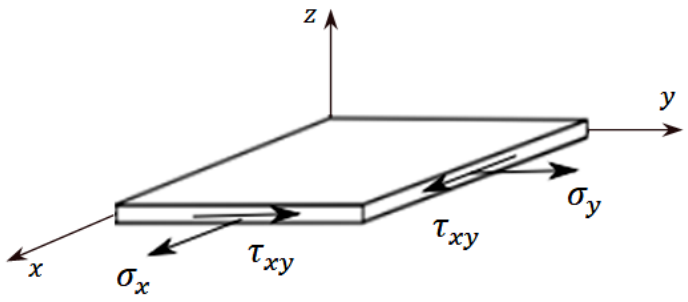

Figure 2.7 *Plane stress state in a thin plate ($\sigma_z = \tau_{zx} = \tau_{zy} = 0$)*

If previous conditions are fulfilled, we can assume that plate, shown in Figure 2.7, is under *plane stress* state. In this case, since: $\sigma_z = \tau_{zx} = \tau_{zy} = 0$, stress tensor has the form:

$$\{\sigma\} = \begin{bmatrix} \sigma_x & \tau_{xy} & 0 \\ \tau_{yx} & \sigma_y & 0 \\ 0 & 0 & 0 \end{bmatrix}. \tag{2.10}$$

While the Hooke's law is given by:

$$\begin{bmatrix} \varepsilon_x \\ \varepsilon_y \\ \varepsilon_z \\ \gamma_{yz} \\ \gamma_{xz} \\ \gamma_{xy} \end{bmatrix} = \begin{bmatrix} S_{11}^{xy} & \cdots & S_{16}^{xy} \\ \vdots & \ddots & \vdots \\ S_{61}^{xy} & \cdots & S_{66}^{xy} \end{bmatrix} \cdot \begin{bmatrix} \sigma_x \\ \sigma_y \\ 0 \\ 0 \\ 0 \\ \tau_{xy} \end{bmatrix}. \tag{2.11}$$

2.2.1 Stress-Strain Relations in a Local Coordinate System

In Figure 2.8 a thin plate made of an orthotropic material is shown where orthogonal axes 1, 2, 3 are principal material axes. These three axes, define three planes of material symmetry: 1–2, 1–3 and 2–3 (see Figure 2.2). Since in such case according to equation (2.7) some compliance constants are equal to zero previous equation (2.11), for orthogonal coordinate system 1–2–3, becomes:

$$\begin{Bmatrix} \varepsilon_1 \\ \varepsilon_2 \\ \varepsilon_3 \\ \gamma_{23} \\ \gamma_{13} \\ \gamma_{12} \end{Bmatrix} = \begin{bmatrix} S_{11} & S_{12} & S_{13} & 0 & 0 & 0 \\ S_{12} & S_{22} & S_{23} & 0 & 0 & 0 \\ S_{13} & S_{23} & S_{33} & 0 & 0 & 0 \\ 0 & 0 & 0 & S_{44} & 0 & 0 \\ 0 & 0 & 0 & 0 & S_{55} & 0 \\ 0 & 0 & 0 & 0 & 0 & S_{66} \end{bmatrix} \begin{Bmatrix} \sigma_1 \\ \sigma_2 \\ 0 \\ 0 \\ 0 \\ \tau_{12} \end{Bmatrix} \tag{2.12}$$

Based on this relationship, it is evident that

$$\gamma_{23} = 0 \qquad \gamma_{13} = 0 \tag{2.13}$$

According to the plane-stress assumption, the occurrence of shear strains is completely absent in planes 2–3 and 1–3. It should be noted that normal strain ε_3 is not independent component of strain since it can be expressed as a function of the other two normal strain ε_1 and ε_2:

$$\varepsilon_3 = S_{13}\sigma_1 + S_{23}\sigma_2 \tag{2.14}$$

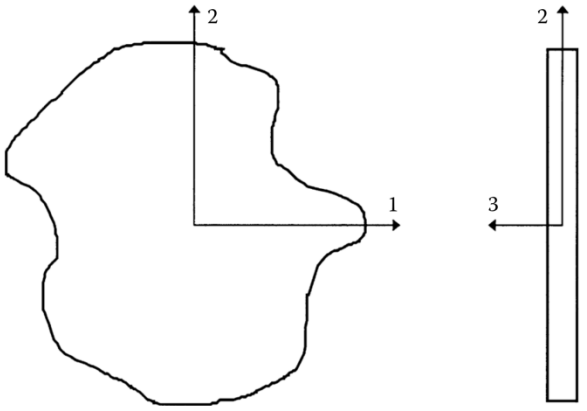

Figure 2.8 *A thin orthotropic plate. Axes 1, 2 and 3 are principal material axes*

The equation (2.14) explicitly demonstrates that in a state of plane stress, an extensional strain in the third direction exists, on the other words, it is incorrect to make the assumption that strain ε_3 is equal to zero. The non-zero nature of the quantity can be attributed to the influence of Poisson's ratios ν_{13} and ν_{23} on S_{13} and S_{23}, respectively, in conjunction with the presence of non-zero stress components σ_1 and σ_2.

Now, Hooke's law for an orthotropic thin plate, for *plane stress* state, defined in orthogonal coordinate system 1–2–3 (where axes 1, 2, 3 are principal material axes defining three planes of material symmetry) can be expressed as:

$$\begin{Bmatrix} \varepsilon_1 \\ \varepsilon_2 \\ \gamma_{12} \end{Bmatrix} = \begin{bmatrix} S_{11} & S_{12} & 0 \\ S_{12} & S_{22} & 0 \\ 0 & 0 & S_{66} \end{bmatrix} \begin{Bmatrix} \sigma_1 \\ \sigma_2 \\ \tau_{12} \end{Bmatrix} = [S] \begin{Bmatrix} \sigma_1 \\ \sigma_2 \\ \tau_{12} \end{Bmatrix} \tag{2.15}$$

As shown in Chapter 2.1.4, compliance matrix coefficients can be defined in terms of appropriate engineering constants as follows:

$$S_{11} = \frac{1}{E_1}, \qquad S_{12} = -\frac{\nu_{12}}{E_1}, \qquad S_{21} = -\frac{\nu_{21}}{E_2}, \qquad S_{22} = \frac{1}{E_2}, \qquad S_{66} = \frac{1}{G_{12}} \tag{2.16}$$

If the plate is made of isotropic material, the previous equation (2.16), simplifies to well known relationships:

$$S_{11} = S_{22} = \frac{1}{E} \qquad S_{12} = -\frac{\nu}{E} \qquad S_{66} = \frac{1}{G} = \frac{2(1+\nu)}{E} \tag{2.17}$$

By the inverse form of the stress-strain relation, equation (2.12), using the plane-stress assumption, becomes:

$$\begin{Bmatrix} \sigma_1 \\ \sigma_2 \\ 0 \\ 0 \\ 0 \\ \tau_{12} \end{Bmatrix} = \begin{bmatrix} C_{11} & C_{12} & C_{13} & 0 & 0 & 0 \\ C_{12} & C_{22} & C_{23} & 0 & 0 & 0 \\ C_{13} & C_{23} & C_{33} & 0 & 0 & 0 \\ 0 & 0 & 0 & C_{44} & 0 & 0 \\ 0 & 0 & 0 & 0 & C_{55} & 0 \\ 0 & 0 & 0 & 0 & 0 & C_{66} \end{bmatrix} \begin{Bmatrix} \varepsilon_1 \\ \varepsilon_2 \\ \varepsilon_3 \\ \gamma_{23} \\ \gamma_{13} \\ \gamma_{12} \end{Bmatrix} \tag{2.18}$$

With the above, it can be concluded that

$$\gamma_{23} = 0 \qquad \gamma_{13} = 0 \tag{2.19}$$

In analogy to equation (2.14), the third equation of equation (2.18) yields

$$0 = C_{13}\varepsilon_1 + C_{23}\varepsilon_2 + C_{33}\varepsilon_3 \tag{2.20}$$

with rearranged, it becomes

$$\varepsilon_3 = -\frac{C_{13}}{C_{33}}\varepsilon_1 - \frac{C_{23}}{C_{33}}\varepsilon_2 \tag{2.21}$$

Equation (2.21) again confirms that ε_3 is not an independent component of strain since it can be expressed as a function of the remaining two linear deformations: i.e. $\varepsilon_3 = f(\varepsilon_1, \varepsilon_2)$.

Similar to how equation (2.12) was reduced to equation (2.15) by eliminating variables, the three-dimensional form of equation (2.18) cannot be reduced directly to a relation involving only σ_1, σ_2, and τ_{12}, and ε_1, ε_2, γ_{12}. The expressions for σ_1 and σ_2 can be established using the first two equations in equation (2.18):

$$\begin{aligned} \sigma_1 &= C_{11}\varepsilon_1 + C_{12}\varepsilon_2 + C_{13}\varepsilon_3 \\ \sigma_2 &= C_{12}\varepsilon_1 + C_{22}\varepsilon_2 + C_{23}\varepsilon_3 \end{aligned} \tag{2.22}$$

When ε_3 is substituted into equation (2.21), the outcome is:

$$\begin{aligned} \sigma_1 &= C_{11}\varepsilon_1 + C_{12}\varepsilon_2 + C_{13}\left(-\frac{C_{13}}{C_{33}}\varepsilon_1 - \frac{C_{23}}{C_{33}}\varepsilon_2\right) \\ \sigma_2 &= C_{12}\varepsilon_1 + C_{22}\varepsilon_2 + C_{23}\left(-\frac{C_{13}}{C_{33}}\varepsilon_1 - \frac{C_{23}}{C_{33}}\varepsilon_2\right) \end{aligned} \tag{2.23}$$

or

$$\begin{aligned} \sigma_1 &= \left(C_{11} - \frac{C_{13}^2}{C_{33}}\right)\varepsilon_1 + \left(C_{12} - \frac{C_{13}C_{23}}{C_{33}}\right)\varepsilon_2 \\ \sigma_2 &= \left(C_{12} - \frac{C_{13}C_{23}}{C_{33}}\right)\varepsilon_1 + \left(C_{22} - \frac{C_{23}^2}{C_{33}}\right)\varepsilon_2 \end{aligned} \tag{2.24}$$

Considering the plane stress state, the relation between stresses and strains can be expressed as follows, which includes the shear stress-shear strain relation:

$$\begin{Bmatrix} \sigma_1 \\ \sigma_2 \\ \tau_{12} \end{Bmatrix} = \begin{bmatrix} Q_{11} & Q_{12} & 0 \\ Q_{12} & Q_{22} & 0 \\ 0 & 0 & Q_{66} \end{bmatrix} \begin{Bmatrix} \varepsilon_1 \\ \varepsilon_2 \\ \gamma_{12} \end{Bmatrix} \tag{2.25}$$

where Q_{ij} are known as the reduced stiffness matrix coefficients. According to equations (2.18) and (2.24) it is clear that there is a difference between the following stiffness matrix coefficients C_{ij} and the following reduced stiffness matrix coefficients Q_{ij} because they are not the same: $Q_{11} \neq C_{11}$, $Q_{12} \neq C_{12}$, $Q_{22} \neq C_{22}$, But, on the other hand $Q_{66} = C_{66}$. Based on equations (2.24) reduced stiffness matrix coefficients Q_{ij} can be expressed in terms of appropriate stiffness matrix coefficients C_{ij} as follows:

$$\begin{aligned} Q_{11} &= C_{11} - \frac{C_{13}^2}{C_{33}} \\ Q_{12} &= C_{12} - \frac{C_{13}C_{23}}{C_{33}} \\ Q_{22} &= C_{22} - \frac{C_{23}^2}{C_{33}} \\ Q_{66} &= C_{66} \end{aligned} \tag{2.26}$$

Reduced stiffness matrix coefficients Q_{ij} are called “reduced” because they are the end outcome of reducing the problem from a completely three-dimensional to a two-dimensional, or plane-stress, problem. It is obvious that equation (2.25) can be obtained by the inverting equation (2.15). By using matrix algebra, it can be proved that reduced stiffness matrix coefficients are related to compliance matrix coefficients in the following form:

$$\begin{aligned} Q_{11} &= \frac{S_{22}}{S_{11}S_{22} - S_{12}^2} \\ Q_{12} &= -\frac{S_{12}}{S_{11}S_{22} - S_{12}^2} \\ Q_{22} &= \frac{S_{11}}{S_{11}S_{22} - S_{12}^2} \\ Q_{66} &= \frac{1}{S_{66}} \end{aligned} \tag{2.27}$$

Based on equation (2.16), after substituting in equation (2.27), reduced stiffness matrix coefficients can be also defined in terms of appropriate engineering constants as follows:

$$
\begin{aligned}
Q_{11} &= \frac{E_1}{1-\nu_{12}\nu_{21}} \\
Q_{12} &= \frac{\nu_{12}E_2}{1-\nu_{12}\nu_{21}} = \frac{\nu_{21}E_1}{1-\nu_{12}\nu_{21}} \\
Q_{22} &= \frac{E_2}{1-\nu_{12}\nu_{21}} \\
Q_{66} &= G_{12}
\end{aligned}
\tag{2.28}
$$

It should be noted that in case when the plate is made of isotropic material the previous equation (2.28) simplifies to well known form:

$$
\begin{aligned}
Q_{11} = Q_{22} &= \frac{E}{1-\nu^2} \qquad\qquad Q_{12} = \frac{\nu E}{1-\nu^2} \\
Q_{66} = G &= \frac{E}{2(1+\nu)}
\end{aligned}
\tag{2.29}
$$

2.2.2 Stress-Strain Relations in a Global Coordinate System

Figure 2.9 shows a thin orthotropic plate where axes 1 and 2 are principal material axes or so-called local axes while the axes x and y are called the global axes or the off-axes. The angle between the local and global axes is denoted by an angle θ. In Figure 2.9 the orientation of angle θ is adopted to be positive. Usually, the stress-strain relations in a global coordinate system can be derived based on static equilibrium of prismatic differential elements *ABC* and *BED* which are cut off from thin orthotropic plate as shown in Figure 2.10. Loads shown in Figure 2.10 are the following stresses: σ_1 and σ_2 are local normal stresses in directions 1 and 2, τ_{12} is shear stress in plane 1–2, while σ_x, and σ_y are global normal stresses in directions x and y while τ_{xy} is shear stress in plane x–y. It can be easily shown that static equilibrium of prismatic differential elements *ABC* and *BED* gives that the global stresses $(\sigma_x, \sigma_y, \tau_{xy})$ and local stresses $(\sigma_1, \sigma_2, \tau_{12})$ are related to each other through the transformation matrix $[T]$:

$$
\begin{bmatrix} \sigma_1 \\ \sigma_2 \\ \tau_{12} \end{bmatrix} = [T] \begin{bmatrix} \sigma_x \\ \sigma_y \\ \tau_{xy} \end{bmatrix}, \tag{2.30}
$$

or in inverted form:

$$
\begin{bmatrix} \sigma_x \\ \sigma_y \\ \tau_{xy} \end{bmatrix} = [T]^{-1} \begin{bmatrix} \sigma_1 \\ \sigma_2 \\ \tau_{12} \end{bmatrix}. \tag{2.31}
$$

where transformation matrix $[T]$ and inverted transformation matrix $[T]^{-1}$ are defined as:

$$[T] = \begin{bmatrix} c^2 & s^2 & 2sc \\ s^2 & c^2 & -2sc \\ -sc & sc & c^2 - s^2 \end{bmatrix}, \qquad [T]^{-1} = \begin{bmatrix} c^2 & s^2 & -2sc \\ s^2 & c^2 & 2sc \\ sc & -sc & c^2 - s^2 \end{bmatrix}, \quad (2.32)$$

where: $c = \cos(\theta), s = \sin(\theta)$ while angle θ is the angle degree between the local and global axis as shown in Figures 2.9 and 2.10.

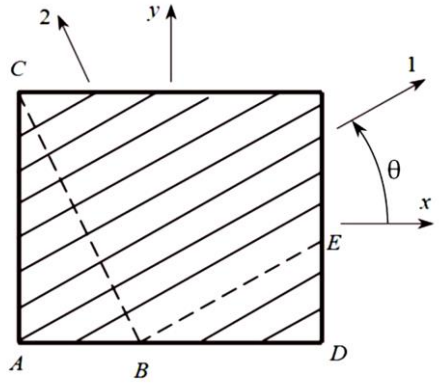

Figure 2.9 *The global (x–y) and local (1–2) coordinate systems of a thin composite plate reinforced with continuous fibers*

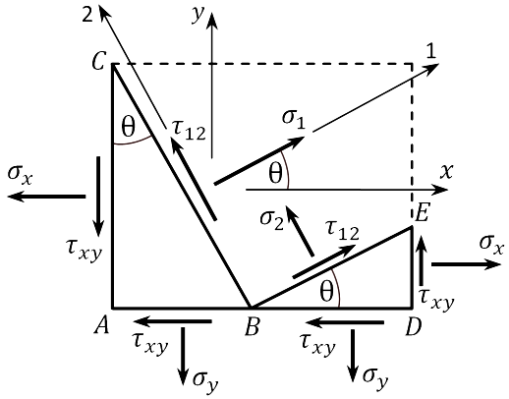

Figure 2.10 *Loads on prismatic differential elements ABC and BED which are cut off from thin orthotropic plate shown in Figure 2.9*

In the same manner, due to the fact that stress and strain are tensors of the same order, the global strains $(\varepsilon_x, \varepsilon_y, \gamma_{xy})$ and local strains $(\varepsilon_1, \varepsilon_2, \gamma_{12})$ in an angle lamina are related to each other through the transformation matrix $[T]$:

$$\begin{bmatrix} \varepsilon_1 \\ \varepsilon_2 \\ \frac{1}{2}\gamma_{12} \end{bmatrix} = [T] \begin{bmatrix} \varepsilon_x \\ \varepsilon_y \\ \frac{1}{2}\gamma_{xy} \end{bmatrix}, \qquad (2.33)$$

or in inverted form:

$$\begin{bmatrix} \varepsilon_x \\ \varepsilon_y \\ \frac{1}{2}\gamma_{xy} \end{bmatrix} = [T]^{-1} \begin{bmatrix} \varepsilon_1 \\ \varepsilon_2 \\ \frac{1}{2}\gamma_{12} \end{bmatrix}, \tag{2.34}$$

where: ε_1 and ε_2 are local normal strains in directions 1 and 2, γ_{12} is the shear strain in plane 1-2, while ε_x and ε_y are global normal strains in directions *x* and *y* while γ_{xy} is the shear strain in plane *x*-*y*. Note that in equations (2.33) and (2.34) the shear strain is multiplied with factor 1/2. To eliminate factor 1/2 in equation (2.33), so-called *Reuter matrix* $[R]$ is introduced:

$$[R] = \begin{bmatrix} 1 & 0 & 0 \\ 0 & 1 & 0 \\ 0 & 0 & 2 \end{bmatrix}. \tag{2.35}$$

After substitution of *Reuter matrix* $[R]$ in the equation (2.33) it can be re-written as:

$$\begin{bmatrix} \varepsilon_1 \\ \varepsilon_2 \\ \gamma_{12} \end{bmatrix} = [R][T][R]^{-1} \begin{bmatrix} \varepsilon_x \\ \varepsilon_y \\ \gamma_{xy} \end{bmatrix}. \tag{2.36}$$

Now, by using equations (2.31), (2.25) and (2.36) it can be shown that the global stresses $(\sigma_x\,, \sigma_y\,, \tau_{xy})$ and the global strains $(\varepsilon_x\,, \varepsilon_y\,, \gamma_{xy})$ are related as follows:

$$\begin{bmatrix} \sigma_x \\ \sigma_y \\ \tau_{xy} \end{bmatrix} = [T]^{-1} \begin{bmatrix} \sigma_1 \\ \sigma_2 \\ \tau_{12} \end{bmatrix} = [T]^{-1}[Q] \begin{bmatrix} \varepsilon_1 \\ \varepsilon_2 \\ \gamma_{12} \end{bmatrix} = [T]^{-1}[Q][R][T][R]^{-1} \begin{bmatrix} \varepsilon_x \\ \varepsilon_y \\ \gamma_{xy} \end{bmatrix}. \tag{2.37}$$

If product of matrix multiplication in equation (2.37) is denoted by matrix $[\bar{Q}]$:

$$[\bar{Q}] = [T]^{-1}[Q][R][T][R]^{-1}, \tag{2.38}$$

then equation (2.37) becomes:

$$\begin{bmatrix} \sigma_x \\ \sigma_y \\ \tau_{xy} \end{bmatrix} = [\bar{Q}] \begin{bmatrix} \varepsilon_x \\ \varepsilon_y \\ \gamma_{xy} \end{bmatrix} = \begin{bmatrix} \bar{Q}_{11} & \bar{Q}_{12} & \bar{Q}_{16} \\ \bar{Q}_{21} & \bar{Q}_{22} & \bar{Q}_{26} \\ \bar{Q}_{61} & \bar{Q}_{62} & \bar{Q}_{66} \end{bmatrix} \begin{bmatrix} \varepsilon_x \\ \varepsilon_y \\ \gamma_{xy} \end{bmatrix}. \tag{2.39}$$

Matrix $[\bar{Q}]$ in equation (2.39) is called *transformed reduced stiffness matrix* while coefficients $\bar{Q}_{kl}$ are called *transformed reduced stiffness matrix coefficients*. These coefficients can be calculated from matrix equation (2.38) as follows:

$$\begin{aligned}
\bar{Q}_{11} &= Q_{11}c^4 + 2(Q_{12} + 2Q_{66})s^2c^2 + Q_{22}s^4 \\
\bar{Q}_{12} &= \bar{Q}_{21} = (Q_{11} + Q_{22} - 4Q_{66})s^2c^2 + Q_{12}(s^4 + c^4) \\
\bar{Q}_{22} &= Q_{11}s^4 + 2(Q_{12} + 2Q_{66})s^2c^2 + Q_{22}c^4 \\
\bar{Q}_{16} &= \bar{Q}_{61} = (Q_{11} - Q_{12} - 2Q_{66})sc^3 - (Q_{22} - Q_{12} - 2Q_{66})s^3c \\
\bar{Q}_{26} &= \bar{Q}_{62} = (Q_{11} - Q_{12} - 2Q_{66})s^3c - (Q_{22} - Q_{12} - 2Q_{66})sc^3 \\
\bar{Q}_{66} &= (Q_{11} + Q_{22} - 2Q_{12} - 2Q_{66})s^2c^2 + Q_{66}(s^4 + c^4)
\end{aligned} \tag{2.40}$$

After inverting, equation (2.39) becomes:

$$\begin{bmatrix}\varepsilon_x\\ \varepsilon_y\\ \gamma_{xy}\end{bmatrix} = [\bar{Q}]^{-1}\begin{bmatrix}\sigma_x\\ \sigma_y\\ \tau_{xy}\end{bmatrix} = [\bar{S}]\begin{bmatrix}\sigma_x\\ \sigma_y\\ \tau_{xy}\end{bmatrix} = \begin{bmatrix}\bar{S}_{11} & \bar{S}_{12} & \bar{S}_{16}\\ \bar{S}_{21} & \bar{S}_{22} & \bar{S}_{26}\\ \bar{S}_{61} & \bar{S}_{62} & \bar{S}_{66}\end{bmatrix}\begin{bmatrix}\sigma_x\\ \sigma_y\\ \tau_{xy}\end{bmatrix}. \qquad (2.41)$$

Matrix $[\bar{S}]$ in equation (2.41) is called *transformed compliance matrix* while coefficients $\bar{S}_{kl}$ are called *transformed compliance matrix coefficients*. Matrices $[\bar{S}]$ and $[\bar{Q}]$ are mutually inverted matrices: $[\bar{S}] = [\bar{Q}]^{-1}$. By using matrix algebra, from equation (2.36), it can be proved that transformed compliance matrix $[\bar{S}]$ can be calculated from:

$$[\bar{S}] = [\mathrm{R}][\mathrm{T}]^{-1}[\mathrm{R}]^{-1}[\mathrm{S}][\mathrm{T}]\,. \qquad (2.42)$$

After substituting expressions for matrices [R], [T] and [S] we obtain transformed compliance matrix coefficients $\bar{S}_{kl}$:

$$\begin{aligned}
\bar{S}_{11} &= S_{11}c^4 + (2S_{12} + S_{66})s^2c^2 + S_{22}s^4\\
\bar{S}_{12} &= \bar{S}_{21} = (S_{11} + S_{22} - S_{66})s^2c^2 + S_{12}(s^4 + c^4)\\
\bar{S}_{22} &= S_{11}s^4 + (2S_{12} + S_{66})s^2c^2 + S_{22}c^4\\
\bar{S}_{16} &= \bar{S}_{61} = (2S_{11} - 2S_{12} - S_{66})sc^3 - (2S_{22} - 2S_{12} - S_{66})s^3c\\
\bar{S}_{26} &= \bar{S}_{62} = (2S_{11} - 2S_{12} - S_{66})s^3c - (2S_{22} - 2S_{12} - S_{66})sc^3\\
\bar{S}_{66} &= 2(2S_{11} + 2S_{22} - 4S_{12} - S_{66})s^2c^2 + S_{66}(s^4 + c^4)
\end{aligned} \qquad (2.43)$$

Compliance matrix coefficients S_{ij} were earlier defined in terms of appropriate engineering constants – see equation (2.16). Therefore, equation (2.43) becomes:

$$\begin{aligned}
\bar{S}_{11} &= \frac{1}{E_1}c^4 + \left[-\frac{2\nu_{12}}{E_1} + \frac{1}{G_{12}}\right]s^2c^2 + \frac{1}{E_2}s^4\\
\bar{S}_{12} &= -\frac{\nu_{12}}{E_1}(s^4 + c^4) + \left[\frac{1}{E_1} + \frac{1}{E_2} - \frac{1}{G_{12}}\right]s^2c^2\\
\bar{S}_{22} &= \frac{1}{E_1}s^4 + \left[-\frac{2\nu_{12}}{E_1} + \frac{1}{G_{12}}\right]s^2c^2 + \frac{1}{E_2}c^4\\
\bar{S}_{16} &= \left[\frac{2}{E_1} + \frac{2\nu_{12}}{E_1} - \frac{1}{G_{12}}\right]sc^3 - \left[\frac{2}{E_2} + \frac{2\nu_{12}}{E_1} - \frac{1}{G_{12}}\right]s^3c\\
\bar{S}_{26} &= \left[\frac{2}{E_1} + \frac{2\nu_{12}}{E_1} - \frac{1}{G_{12}}\right]s^3c - \left[\frac{2}{E_2} + \frac{2\nu_{12}}{E_1} - \frac{1}{G_{12}}\right]sc^3\\
\bar{S}_{66} &= 2\left[\frac{2}{E_1} + \frac{2}{E_2} + \frac{4\nu_{12}}{E_1} - \frac{1}{G_{12}}\right]s^2c^2 + \frac{1}{G_{12}}(s^4 + c^4)
\end{aligned} \qquad (2.44)$$

The strains of an orthotropic thin plate material element, as measured in the *x*-*y*-*z* global coordinate system, are related to the applied stresses, according to equations (2.39) and (2.41). From a purely linear algebraic perspective, we can see that these equations are the end result of basic operations like transformations and inversions. Equation (2.41) states that a normal stress σ_x will produce shearing deformation γ_{xy} via the $\bar{S}_{16}$ term, and a normal stress σ_y will do the same through the $\bar{S}_{26}$ term. Shear stress τ_{xy} will cause strains ε_x and ε_y, due to the presence of these same terms, $\bar{S}_{16}$ and $\bar{S}_{26}$. Therefore, it is obvious that shear-extension coupling effect exists. The term shear-extension coupling refers to the coupling found in anisotropic materials (e.g. fiber reinforced composites). This material behaviour is utterly dissimilar to the ones found in isotropic materials (e.g. metals).

It should be noted that $\bar{S}_{12}$ and all terms on the diagonal are symmetrical functions of θ (mirrored at θ = 0° and repeated every 90°), whereas the off-diagonal terms $\bar{S}_{16}$ and $\bar{S}_{26}$ are asymmetrical functions of θ. Thus, when θ = 0° equation (2.44) simplifies to:

$$\begin{aligned} &\bar{S}_{11}(0°) = S_{11} && \bar{S}_{22}(0°) = S_{22} \\ &\bar{S}_{12}(0°) = S_{12} && \bar{S}_{26}(0°) = 0 \\ &\bar{S}_{16}(0°) = 0 && \bar{S}_{66}(0°) = S_{66} \end{aligned} \tag{2.45}$$

The result of equation (2.45), is logical since case when θ = 0° refers to the principal material coordinate system. None of the $\bar{S}_{16}$ or $\bar{S}_{26}$ exist in the principal material system. The off-axis compliances are a common name for the barred quantities in equation (2.44).

It should be noted that in case when the plate is made of isotropic material the previous equation (2.44) simplifies to:

$$\begin{aligned} \bar{S}_{11} &= \frac{1}{E} \\ \bar{S}_{22} &= \frac{1}{E} \\ \bar{S}_{12} &= -\frac{\nu}{E} \\ \bar{S}_{16} &= 0 \\ \bar{S}_{26} &= 0 \\ \bar{S}_{66} &= \frac{1}{G} = \frac{2(1+\nu)}{E} \end{aligned} \tag{2.46}$$

2.3 Elastic Constants in a Global Coordinate System

The elastic constants related to the 1–2–3 principal material coordinate system (E_1, E_2, etc.) were introduced in Chapter 2.1.4. Based on that discussion the elastic constants of the thin orthotropic plate for global coordinate system x–y can be directly derived from their definitions.

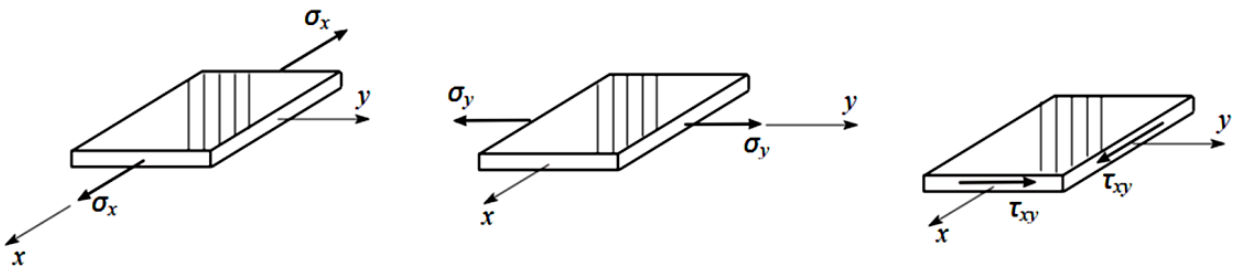

(a) (b) (c)

Figure 2.11 *Off-axis element with simple stress states for definition of elastic constants*

Take into consideration, as shown in Figure 2.11 (a), an off-axis element of the orthotropic thin plate in the x–y coordinate system with its fiber oriented at some angle θ with respect to the x axis. The element is subjected to a normal tensile stress σ_x while all other stresses are set to zero while the magnitude of the tensile stress is up to elastic limit. Now, equation (2.41) becomes:

$$\begin{bmatrix} \varepsilon_x \\ \varepsilon_y \\ \gamma_{xy} \end{bmatrix} = \begin{bmatrix} \bar{S}_{11} & \bar{S}_{12} & \bar{S}_{16} \\ \bar{S}_{12} & \bar{S}_{22} & \bar{S}_{26} \\ \bar{S}_{16} & \bar{S}_{26} & \bar{S}_{66} \end{bmatrix} \begin{bmatrix} \sigma_x \\ 0 \\ 0 \end{bmatrix}, \tag{2.47}$$

or,

$$\varepsilon_x = \bar{S}_{11}\sigma_x \ , \tag{2.48}$$
$$\varepsilon_y = \bar{S}_{12}\sigma_x \ , \tag{2.49}$$
$$\gamma_{xy} = \bar{S}_{16}\sigma_x \ , \tag{2.50}$$

resulting in existence of all components of strain. In response to this applied stress, the element stretches in the x direction, expected to contracts in the y direction, and because the x–axis is not aligned with principal material direction 1, the shear strain γ_{xy} arise. By definition of the Hooke's law, extensional strain in the x direction (ε_x) is related to the stress in the x direction (σ_x) by the elasticity modulus in the x direction (E_x):

$$\varepsilon_x = \frac{\sigma_x}{E_x} \tag{2.51}$$

However, from the strain-stress relations of equation (2.48) extensional strain in the x direction (ε_x) is:

$$\varepsilon_x = \bar{S}_{11}\sigma_x \tag{2.52}$$

since previous two equations are identic, the elasticity modulus in the x direction (E_x) is obtained to be:

$$E_x = \frac{1}{\bar{S}_{11}} \tag{2.53}$$

Due to Poisson's effect when the orthotropic thin plate element shown in Figure 2.11 (a) is subjected to a tensile stress in the x direction, it not only stretches in that direction, but it also contracts in the y direction. By the definition Poisson's ratio ν_{xy} is the following quotient:

$$\nu_{xy} = -\frac{\varepsilon_y}{\varepsilon_x} \tag{2.54}$$

where the first subscript indicates the direction of the applied stress, while the second subscript indicates the direction of contraction. From the strain-stress relations of equation (2.49) extensional strain in the y direction (ε_y) is:

$$\varepsilon_y = \bar{S}_{12}\sigma_x \tag{2.55}$$

By substituting equations (2.52) and (2.55) into equation (2.54) Poisson's ratio ν_{xy} is:

$$\nu_{xy} = -\frac{\bar{S}_{12}}{\bar{S}_{11}} \tag{2.56}$$

According to Lekhnitskii, *the coefficients of the mutual influence of the first kind*: $m_{x,xy}$ and $m_{y,xy}$ represent the effect of anisotropy in the $x-y$ plane in terms of the appearance of strains in the directions of the x and y axes ($\varepsilon_x, \varepsilon_y$) due to the shear stress τ_{xy} (where: $\sigma_x = \sigma_y = 0$), while the coefficients of mutual influence of the second kind: $n_{xy,x}$ and $n_{xy,y}$ represent the occurrence of shear strain in the $x-y$ plane (γ_{xy}) due to the action of normal stresses σ_x (where: $\sigma_y = \tau_{xy} = 0$) and σ_y (where $\sigma_x = \tau_{xy} = 0$). In a similar way as Poisson's coefficient couples linear strains, coefficients of mutual influence couple linear and shear strains. By the definition *coefficient of mutual influence of the second kind*: $n_{xy,x}$ is:

$$n_{xy,x} \equiv -\frac{\gamma_{xy}}{\varepsilon_x} \quad (\sigma_x \neq 0) \tag{2.57}$$

From equation (2-48) shear strain is:

$$\gamma_{xy} = \bar{S}_{16}\sigma_x \ , \tag{2-58}$$

By substituting equations (2.48) and (2.58) into equation (2.57) the coefficient of mutual influence of the second kind: $n_{xy,x}$ is:

$$n_{xy,x} = -\frac{\bar{S}_{16}}{\bar{S}_{11}} \tag{2.59}$$

The conditions shown in Figure 2.11 (b), correspond to what happens when a normal stress in the y direction (σ_y) is applied to the orthotropic thin plate element instead of a stress σ_x. In case when only normal stress σ_y is applied, equation (2.41) becomes:

$$\begin{bmatrix} \varepsilon_x \\ \varepsilon_y \\ \gamma_{xy} \end{bmatrix} = \begin{bmatrix} \bar{S}_{11} & \bar{S}_{12} & \bar{S}_{16} \\ \bar{S}_{12} & \bar{S}_{22} & \bar{S}_{26} \\ \bar{S}_{16} & \bar{S}_{26} & \bar{S}_{66} \end{bmatrix} \begin{bmatrix} 0 \\ \sigma_y \\ 0 \end{bmatrix}, \tag{2.60}$$

or,

$$\varepsilon_x = \bar{S}_{12}\sigma_y \ , \tag{2.61}$$
$$\varepsilon_y = \bar{S}_{22}\sigma_y \ , \tag{2.62}$$
$$\gamma_{xy} = \bar{S}_{26}\sigma_y \ , \tag{2.63}$$

resulting again in existence of all components of strain. By definition of The Hooke's law extensional strain in the y direction (ε_y) is related to the normal stress in the y direction (σ_y) by the elasticity modulus in the y direction (E_x):

$$\varepsilon_y = \frac{\sigma_y}{E_y} \tag{2.64}$$

Since equations (2.62) and (2.64) are identic, the elasticity modulus in the y direction (E_y) is:

$$E_y = \frac{1}{\bar{S}_{22}} \tag{2.65}$$

By the definition Poisson's ratio ν_{yx} is the following quotient:

$$\nu_{yx} = -\frac{\varepsilon_x}{\varepsilon_y} \tag{2.66}$$

By substituting equations (2.61) and (2.62) into equation (2.66) Poisson's ratio ν_{yx} is:

$$\nu_{yx} = -\frac{\bar{S}_{12}}{\bar{S}_{22}} \tag{2.67}$$

Based on previous discussion, it can be easily proved that in case of the orthotropic thin plate element the following dependencies must be fulfilled:

$$\frac{\nu_{xy}}{E_x} = \frac{\nu_{yx}}{E_y} .$$

By the definition coefficient of mutual influence of the second kind: $n_{xy,y}$ is:

$$n_{xy,x} \equiv -\frac{\gamma_{xy}}{\varepsilon_y} \quad (\sigma_y \neq 0) \tag{2.68}$$

By substituting equations (2.62) and (2.63) into equation (2.68) the coefficient of mutual influence of the second kind: $n_{xy,x}$ is:

$$n_{xy,y} = -\frac{\bar{S}_{16}}{\bar{S}_{22}} \tag{2.69}$$

Finally, the conditions shown in Figure 2.11 (c), correspond to what happens when a shear stress in the $x-y$ plane (τ_{xy}) is applied to the orthotropic thin plate element. In case when only shear stress τ_{xy} is applied, equation (2.41) becomes:

$$\begin{bmatrix} \varepsilon_x \\ \varepsilon_y \\ \gamma_{xy} \end{bmatrix} = \begin{bmatrix} \bar{S}_{11} & \bar{S}_{12} & \bar{S}_{16} \\ \bar{S}_{12} & \bar{S}_{22} & \bar{S}_{26} \\ \bar{S}_{16} & \bar{S}_{26} & \bar{S}_{66} \end{bmatrix} \begin{bmatrix} 0 \\ 0 \\ \tau_{xy} \end{bmatrix}, \tag{2.70}$$

or,

$$\varepsilon_x = \bar{S}_{16}\tau_{xy} , \tag{2.71}$$
$$\varepsilon_y = \bar{S}_{26}\tau_{xy} , \tag{2.72}$$
$$\gamma_{xy} = \bar{S}_{66}\tau_{xy} , \tag{2.73}$$

resulting again in existence of all components of strain. By definition of extended Hooke's law shear strain in the $x-y$ plane (γ_{xy}) is related to the shear stress τ_{xy} by the shear modulus in the $x-y$ plane (G_{xy}):

$$\gamma_{xy} = \frac{\tau_{xy}}{G_{xy}} \tag{2.74}$$

Since equations (2.73) and (2.74) are identic, the shear modulus in the $x-y$ plane $\left(G_{xy}\right)$ is:

$$G_{xy} = \frac{1}{\bar{S}_{66}} \tag{2.75}$$

Based on previous discussion, having in mind the definition of the coefficients of the mutual influence of the first kind $m_{x,xy}$ and $m_{y,xy}$:

$$m_{x,xy} \equiv -\frac{\varepsilon_x}{\gamma_{xy}} \ \left(\tau_{xy} \neq 0\right) , \qquad m_{y,xy} \equiv -\frac{\varepsilon_y}{\gamma_{xy}} \ \left(\tau_{xy} \neq 0\right) ,$$

it can be easily proved that in case of the orthotropic thin plate element the following dependencies must be fulfilled:

$$\frac{n_{xy,x}}{E_x} = \frac{m_{x,xy}}{G_{xy}} ,$$

$$\frac{n_{xy,y}}{E_y} = \frac{m_{y,xy}}{G_{xy}} .$$

Based on equations (2.53), (2.56), (2.59), (2.65), (2.69) and (2.75) transformed compliance matrix coefficients $\bar{S}_{kl}$ can be expressed in terms of elastic constants related to global coordinate system x–y as follows:

$$\begin{aligned} &\bar{S}_{11} = \frac{1}{E_x} , \ \bar{S}_{12} = -\frac{\nu_{xy}}{E_x} , \ \bar{S}_{22} = \frac{1}{E_y} , \ \bar{S}_{66} = \frac{1}{G_{xy}} , \\ &\bar{S}_{16} = -\frac{n_{xy,x}}{E_x} , \quad \bar{S}_{26} = -\frac{n_{xy,y}}{E_y} . \end{aligned} \tag{2.76}$$

In previous Chapter 2.2.2 we obtained transformed compliance matrix coefficients $\bar{S}_{kl}$ in terms of appropriate engineering constants - see equation (2.44). By combining equations (2.44) and (2.76) we obtain:

$$\frac{1}{E_x} = \frac{1}{E_1}c^4 + \left[-\frac{2\nu_{12}}{E_1} + \frac{1}{G_{12}}\right]s^2c^2 + \frac{1}{E_2}s^4 , \tag{2.77}$$

$$\frac{\nu_{xy}}{E_x} = \frac{\nu_{12}}{E_1}(s^4 + c^4) - \left[\frac{1}{E_1} + \frac{1}{E_2} - \frac{1}{G_{12}}\right]s^2c^2 , \tag{2.78}$$

$$\frac{1}{E_y} = \frac{1}{E_1}s^4 + \left[-\frac{2\nu_{12}}{E_1} + \frac{1}{G_{12}}\right]s^2c^2 + \frac{1}{E_2}c^4 , \tag{2.79}$$

$$\frac{n_{xy,x}}{E_x} = -\left[\frac{2}{E_1} + \frac{2\nu_{12}}{E_1} - \frac{1}{G_{12}}\right]sc^3 + \left[\frac{2}{E_2} + \frac{2\nu_{12}}{E_1} - \frac{1}{G_{12}}\right]s^3c , \tag{2.80}$$

$$\frac{n_{xy,y}}{E_y} = -\left[\frac{2}{E_1} + \frac{2\nu_{12}}{E_1} - \frac{1}{G_{12}}\right]s^3c + \left[\frac{2}{E_2} + \frac{2\nu_{12}}{E_1} - \frac{1}{G_{12}}\right]sc^3 , \tag{2.81}$$

$$\frac{1}{G_{xy}} = 2\left[\frac{2}{E_1} + \frac{2}{E_2} + \frac{4\nu_{12}}{E_1} - \frac{1}{G_{12}}\right]s^2c^2 + \frac{1}{G_{12}}(s^4 + c^4) . \tag{2.82}$$

The above equations actually define the *off-axis engineering properties* of the orthotropic thin plate element.

3 FDM fabricated plate-like parts from PET-G polymer reinforced with short carbon fibers

As earlier mentioned, the resulting properties of a composite material in general depend on the properties of the individual constituents, but also their geometry and the dispersion of phases. Details on possible geometries of the reinforcements used in composites are already outlined in the Introduction of this thesis (see Figure 1.2). From this Chapter and further on throughout the thesis, Short Carbon Fibers (SCF) are particularly interesting as these were used as reinforcements of the here-studied polymeric plate-parts. PET-G filament from Black Element with claimed 30% weight fraction of SCF was used for preparing the plate-like parts for the study. Therefore, studied polymeric samples are actually reinforced with the discontinuous fibers and CLT principles cannot be directly applied to predict their behaviour without previous research into their behaviour under relevant loadings – in this thesis the in-plane ones are in focus. It is also noteworthy that additive manufacturing as a production technique selected to fabricate the studied samples influences the distribution of the discontinuous fibers used as reinforcements which determines the homogeneity (uniformity) of the material system. The more non-uniform the reinforcement distribution, the more heterogeneous the material, and the higher the scatter in properties and the probability of failure in the weakest areas [1]. On top of that, the orientation of the reinforcement is known to affect the mechanical behaviour and occurrence of the anisotropy of the material system and therefore the raster angle potentially defining the in-plane angle of reinforcement orientation within the additively manufactured plates is chosen to be further examined.

3.1 Short carbon fibers as reinforcements in additively manufactured parts

Composite filaments with a polymer matrix and microscale additives were developed to enhance the strength and stiffness properties of additively manufactured parts – i.e. to bridge the gap in terms of mechanical properties between continuous fiber reinforced composites and unreinforced polymers used in everyday applications [30]. Short carbon fibers (SCF) are primarily used as the advantageous reinforcing agents. Particularly, the milled carbon fibers (around 200 μm long) are added to polymer matrix to form a sort of composite filament material utilised for 3D printing and fabricating the composite parts as well. The selection of the reinforcing additive and a proper polymer matrix is an issue directly dependant on the type of application the produced part is intended for. Hence, there should be noted that the PET-G polymer reinforced with SCF selected for this study might be used for parts intended for moderate loadings, but bearing in mind that this material is a low cost one and at the same time available and easy to process on an affordable desktop 3D printer.

Additive composites infused with SCF have been successfully produced and are readily available on the market. Yet, a complete understanding of their behaviour under load remains a respectable area of research, given the morphological inhomogeneities present in the final additively manufactured part which influence the desired and pre-tailored mechanical properties. In order to obtain the stereological reconstructions and visualization of 3D models of the two-phase composite structure, micro-CT X-ray images may be used. For example, Lobov et al. [26] reconstructed a model of a monofilament sample 3D-printed from

acrylonitrile butadiene styrene (ABS) filled with SCF shown in Figure 3.1. There can be seen that SCF within ABS polymer are mainly oriented along with the printing direction (along vertical in the depicted model).

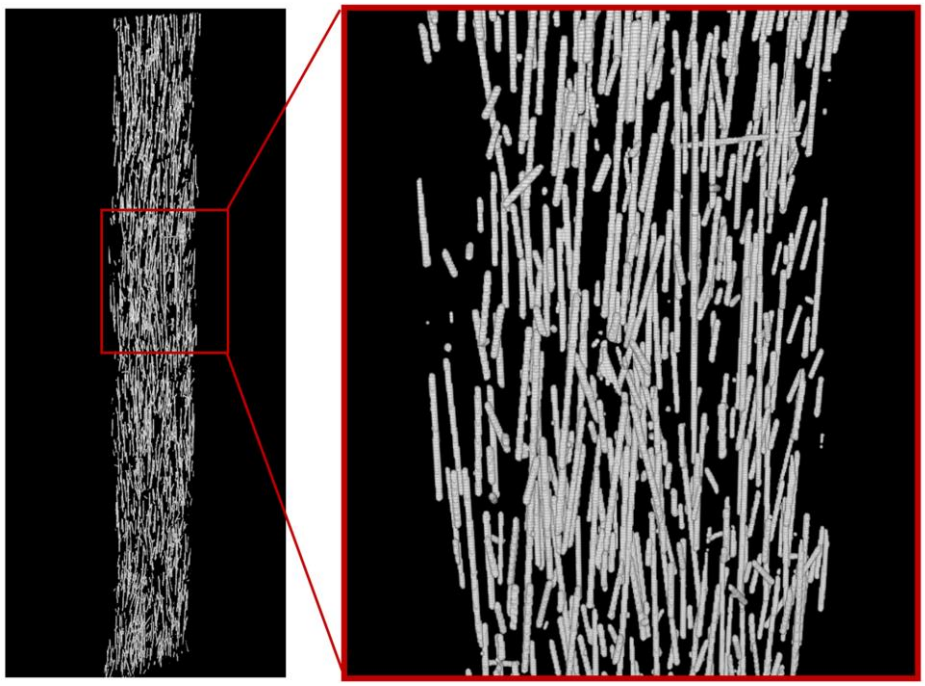

Figure 3.1 *Model of the SCF reinforcement structure of a single-layer monofilament sample (general view and enlarged fragment) obtained from micro-CT data [26]*

3.2 Raster angle as the influential parameter in FDM

Alongside other FDM process parameters such as build orientation, layer thickness, infill density, extrusion width or nozzle temperature, the printing direction commonly referred to as "raster angle" appear to be one of the main parameters when influence on final mechanical properties is considered, especially for parts printed with flat orientation [8, 18]. Raster angle θ is the angle between the direction of the deposited beads and the x-axis (axis of load application), as shown in Figure 3. 2.

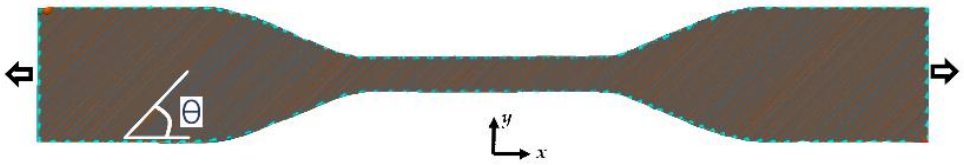

Figure 3.2 *Schematic of raster angle (θ) in a 3D printed part [32]*

The importance of the applied raster angle while printing the short fiber reinforced parts becomes obvious if this angle at the same time determines the angle of spreading the introduced reinforcements. This cannot be undoubtedly said to be true in advance as it is the case with the continuous fibers used as reinforcements. Again, there should be stated that in order to reach the full potential of FDM as an effective and versatile fabrication method to get the load-

bearing structural components, imbedding reinforcements such as continuous or short fibers, particles and nanomaterials into the polymer matrix is required. Only for the first ones, namely continuous fiber reinforced composites, there are available relations that might be applied to the fabricated parts with more or less adjustment – relations already known from CLT. Recently, numerous researchers opted for short carbon fibers as reinforcements to improve the mechanical properties of the FDM based additive parts because of commercial availability of the feedstock materials and ease of fabrication. For instance, it is noted that short carbon fibers used as fillers within the epoxy-based matrix tend to orient along the printing direction due to the shear stress induced in the extrusion process around the print nozzle [7] – see Figure 3.3. As for more common polymers in 3D printing like ABS, the effects of raster angle on mechanical behaviour of parts fabricated from commercially available composite filaments seem to still be unknown and in that context Iyer et al. [29] report the effects of raster angle on the tensile strength, elastic modulus, flexural strength, flexural modulus, and fracture toughness of FDM SCF-reinforced ABS. A decreasing trend in tensile and flexural mechanical properties with increasing raster angle was observed.

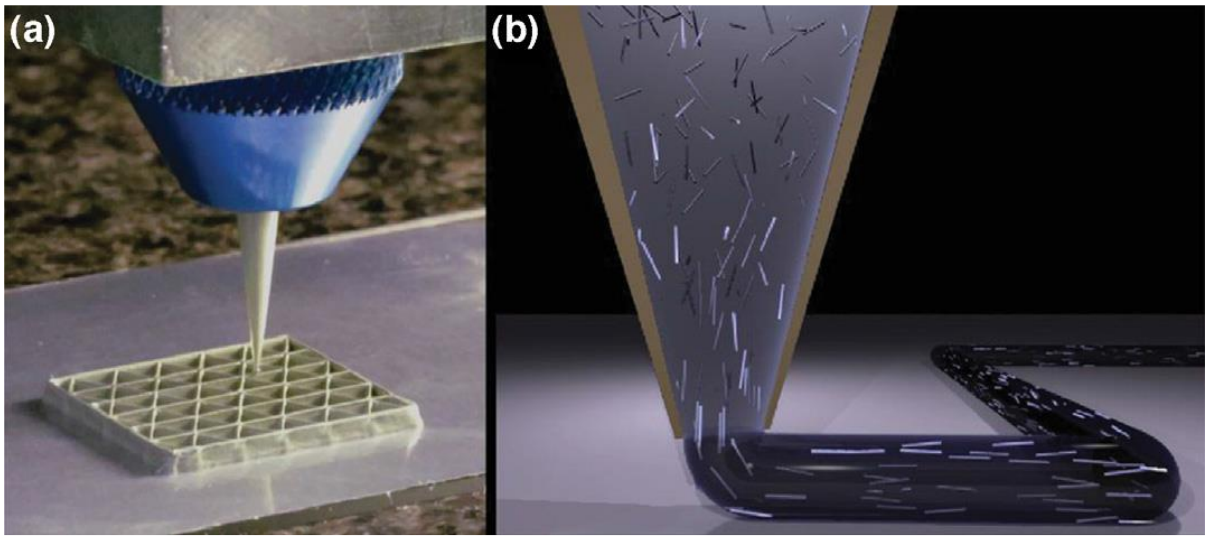

Figure 3.3 *(a) FDM process; (b) Schematic of fiber orientation within epoxy-based resin [7, 33]*

4 Experimental procedure and results

The test specimens fabricated from PET-G material reinforced with short carbon fibers (SCF) are investigated for their tensile properties. For the fabrication process, a flat build orientation was used. Experimental assessments of ultimate tensile strength and stiffness are conducted for specimens manufactured with raster angles varying from 0° to 90°, with a 15° increment.

4.1 Sample specifications and printing parameters

The printing of tensile test specimens adheres to ASTM D638-03 standard [35] - the Type I specimens.

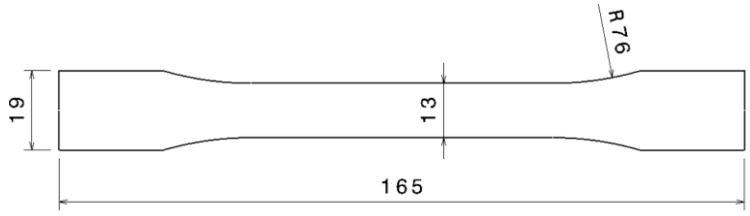

Figure 4.1 *TYPE I Specimen Dimensions: Length overall 165mm, Width of narrow section 13mm, Width overall 19mm, Radius of fillet 76mm*

A steel nozzle was utilized to guarantee wear resistance due to the extremely abrasive nature of carbon fiber reinforced filaments. The nozzle had a diameter of 0.4 mm. Prusa MINI+ 3D printer settings used to create the test specimens included a heated bed temperature of 90°C, a speed of 80 mm/s, an extrusion width of 0.45 mm, a layer thickness of 0.2 mm and an infill density of 100% with 25% overlapping (to keep the air gap to a minimum). It is common for two neighbouring rasters (beads) to have an air gap, i.e. captured air. Although overlapping can lead to uneven surfaces, longer printing times and dimensional inequality, it can also reduce the air gap, enhance the part's integrity and make diffusions between neighbouring layers easier [27, 28]. For the purpose of avoiding any additional impact on the mechanical properties of the final product, all of the specimens were printed without contour lines.

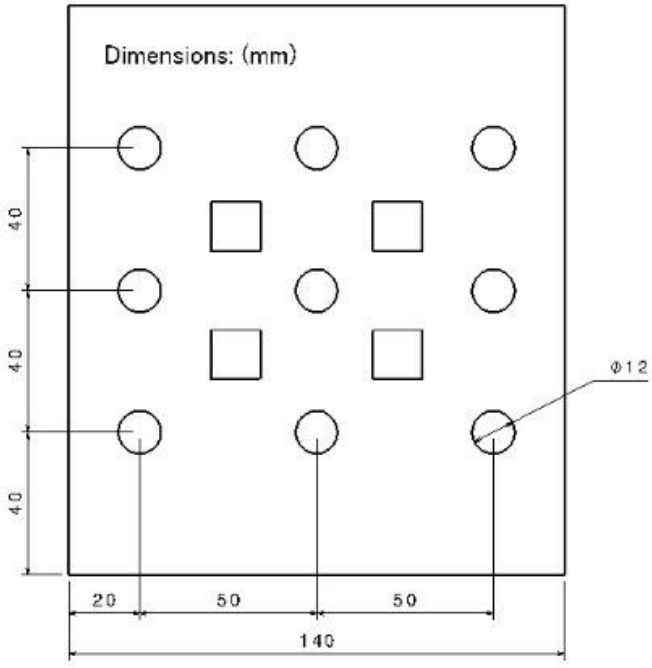

Figure 4.2 *Procedure B, Three-Rail Shear Specimen, SI Units*

Dimensions of specimens printed for shear testing (Figure 4.2) are in accordance with ASTM D4255 standard [36]. This test method determines the in-plane shear properties of fiber reinforced composite materials in general, by either of two procedures. The *Three-Rail Shear Test* procedure is utilised here (see also Figures 4.12 and 4.13). All printing parameters were set to be the same as for the specimens printed for tensile testing. Thickness of the specimens was 3 mm and all the specimens were printed in a way that extruded material lines are deposited transversely (along the shorter side of the specimen shown in Figure 4.2) which corresponds to the 90° raster angle if using the previously defined terminology for the tensile test specimens.

4.2 Tensile testing and obtained results

For each of the raster angles that were considered (0°, 15°, 30°, 45°, 60°, 75° and 90°) series of five test specimens were printed – see Figure 4.3. PET-G filament with manufacturer claimed 30% weight fraction of SCF used for printing the specimens was produced by *Black Element*, China.

Tensile tests were conducted on the Shimadzu AG-Xplus universal testing machine (Figure 4.4). The results encompassing applied force and current elongation were continuously recorded and monitored through the built-in software -Trapezium X. A testing speed of 2.5 mm/min was used. Digital Image Correlation (DIC) was used to record the extensional strain rates of samples during the actual test on the universal testing machine. The fracture surfaces of the tested specimens were then analyzed using scanning electron microscopy (SEM).

Figure 4.3 *Set of printed samples prepared for tensile testing*

Figure 4.4 *Experimental setup used for the tensile test*

4.2.1 Universal testing machine results

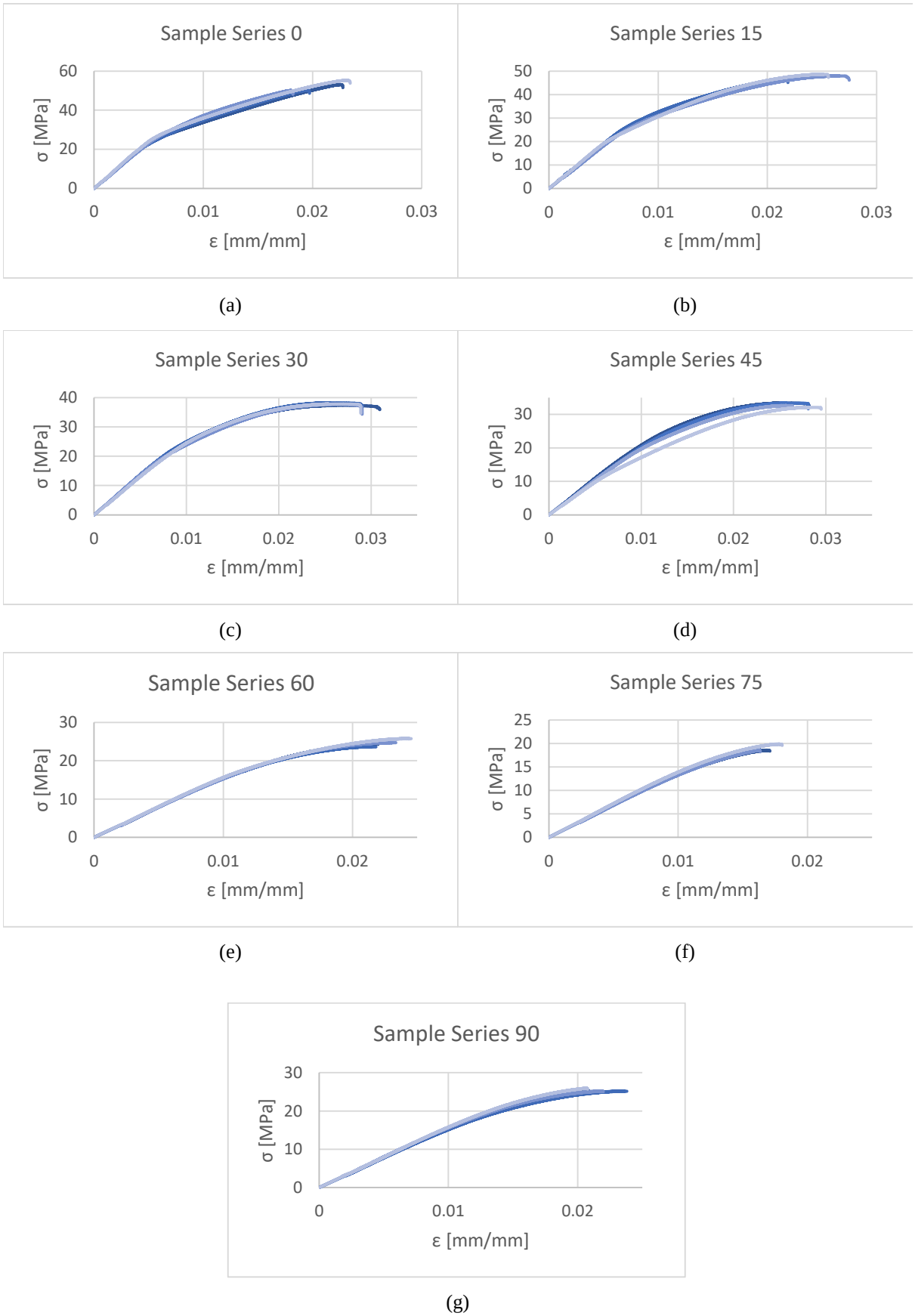

Figure 4.5 *Stress-strain curves obtained for different sample series defined by raster angle*

Figure 4.6 shows the series-averaged stress-strain diagrams altogether, generated from the data collected by the tensile testing conducted on the universal testing machine (previously depicted through Figure 4.5 for particular sample series). The stress-strain curves clearly show that the tested samples initially exhibited linear-elastic behaviour. The transition between the elastic and inelastic regions on the stress-strain curves is not so clearly defined for all the sample series tested. The fracture of all samples occurred shortly after reaching their ultimate tensile strength.

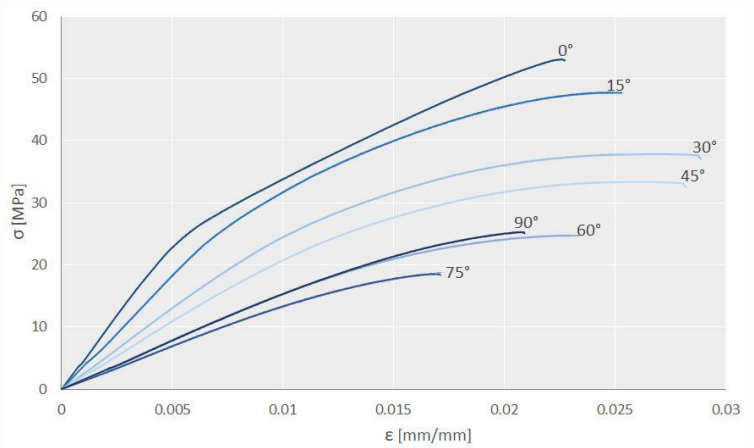

Figure 4.6 *Stress-strain curves for different raster angles [32]*

The process which ensures the corrected zero point on the strain axis (namely toe compensation) was performed on the original stress-strain curves derived from universal testing machine results. This process ensures that the recorded strain values are accurately displayed.

Figure 4.7a shows a bar graph that highlights the variation in the modulus of elasticity values computed for various raster angles. As compared to specimens printed applying the 60°, 75° and 90° raster angles, the 0° raster angle specimen obviously ensures considerably higher stiffness property. For that reason, it's clear that raster angle changes cause mechanical anisotropy occurrence. Figure 4.7b outlines the average values of the ultimate tensile strength obtained for different raster angles. The strength values were found to be highest for samples printed with 0° raster angle and lowest for samples printed with 75° raster angle. The anisotropic property of the tested material explains why samples printed with 75° raster angle delivered a minimum ultimate tensile strength value, even though a minimum value for samples printed with a 90° raster angle was initially anticipated.

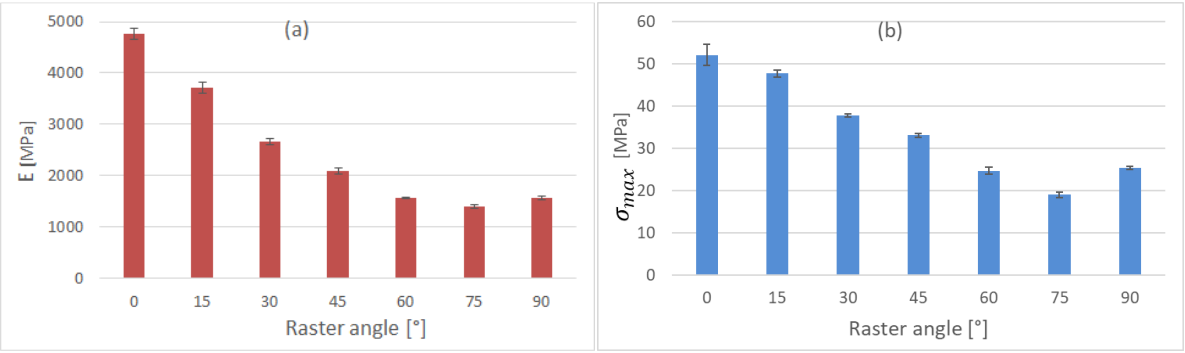

Figure 4.7 *Variation of modulus of elasticity (a) and ultimate tensile strength (b) with change in raster angle*

4.2.2 DIC results

The Digital Image Correlation (DIC) is a non-contact measuring method which enables the assessment of the deformation characteristics of the object observed. Actually, it is a displacement measurement technique. Displacement is measured by defining and tracking markers or patterns on the object's surface. This is achieved by comparing digital images of the object taken before, during and after the deformation. By comparing the positions of these markers in images captured before, during and after the deformation, the software gathers information about the displacements at various points on the object. These data are used afterwards to calculate corresponding strain values.

In this experimental testing, the specimens' deformations were monitored by DIC measuring system ARAMIS from GOM Metrology. Before the actual test, specimens were prepared by applying a stochastic white/black spray pattern onto the surfaces to be recorded. During the test, ARAMIS recognizes the surface structure of the measured object in digital camera images and allocates coordinates to the image pixels. Then, in the measuring project, the image taken initially as the reference one (e.g. see Figure 4.8a) represents the undeformed state of the object. During the deformation of the observed specimen, further images are recorded (e.g. see Figure 4.8b) and then are compared to calculate the necessary displacements.

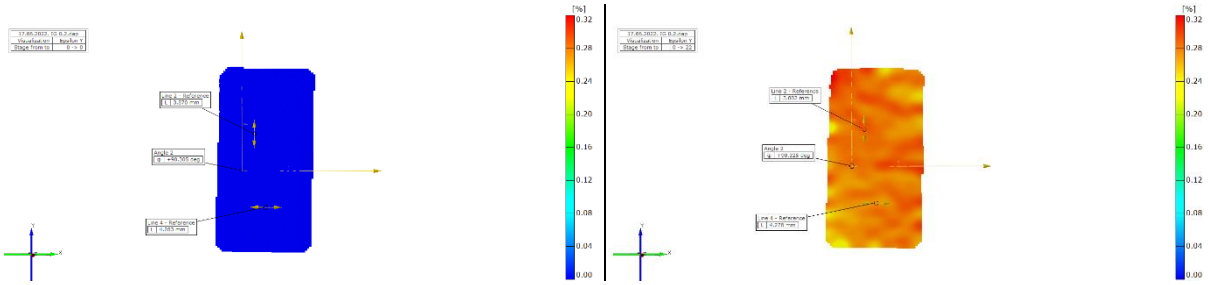

Figure 4.8 *An example of recorded a) initial reference condition (no deformation) and b) during the deformation (stage within the linear elastic region took as a second reference) of the 0° raster angle specimen*

In order to accurately calculate normal strains ($\varepsilon_x, \varepsilon_y$) and in-plane shear strain (γ_{xy}), linear and angular displacements of certain reference points within the gauge section of the specimens were tracked throughout the recorded stages (like using virtual strain gauges – see Figure 4.8). The same time stages were taken for all the specimens so the results could be comparable – the no deformation stage as the first one and the stage where all the examined specimens are still in the linear elastic region as the second one. These displacement data (linear ones in the longitudinal and transverse direction, as well as the angular ones) are then compared for the two chosen stages and corresponding strains are calculated. Obtained values for specimens printed with different raster angles are given in Table 4.1.

Table 4.1 *Summary of values calculated for normal and shear strains for different raster angles*

Raster angle [°]	ε_x [mm/mm]	ε_y [mm/mm]	γ_{xy} [°]
0	-0.00117	0.00310	-0.008
30	-0.00125	0.00387	-0.191
45	-0.00134	0.00386	-0.106
60	-0.00025	0.00309	-0.062
90	-0.00025	0.00387	-0.008

4.2.3 SEM results

The Scanning Electron Microscope (SEM) is an instrument that can produce a largely magnified image of the observed specimen's surface by using electrons instead of light to form an image. It is a type of electron microscope that uses a focused beam of electrons. Therefore, it implies a technique used to obtain high-resolution images and detailed information about the specimen surface. Because of that, it is suitable for materials characterization and research at the sub-micron scale.

For the conducted experiment, Tescan Mira 3 SEM was used to obtain the magnified images of the specimens' fracture surfaces for a closer observation. After tensile testing, specimens were cut to fit the SEM chamber and placed in a way that the fracture surface faces the electron source in order to closely inspect the fracture surfaces under SEM.

Fracture surfaces of the specimens printed with the 0° and 90° raster angles were recorded using SEM, as shown in Figures 4.9 and 4.10. Recorded SEM images allowed for examination of the specimens' inhomogeneity in the fracture zone region, together with orientation of the introduced short carbon fibers in relation to the applied printing direction.

Figure 4.9a presents the fracture surface of the specimen printed with the 0° raster angle revealing the cross section of one raster and air gap formed around it. The yellow circles emphasise some of the carbon fibers that were captured. The dimension of 425 μm highlighted in Figure 4.9a which is a measure of the raster width, corresponds to the preassigned printing parameter (extrusion width). There can also be noticed that the fibers are mostly aligned with the direction of the printing (direction of depositing the beads). In case depicted in Figure 4.9a fibers are pointing out of the image (direction normal to image plane). The orientation of short carbon fibers and the fibers themselves are more clearly visible in Figure 4.9b. Therefore, it is proved that short carbon fibers used as reinforcements generally align within the flow of printing direction and this could be the main reason why specimens fabricated with the 0° raster angle exibited the highest value of ultimate strength.

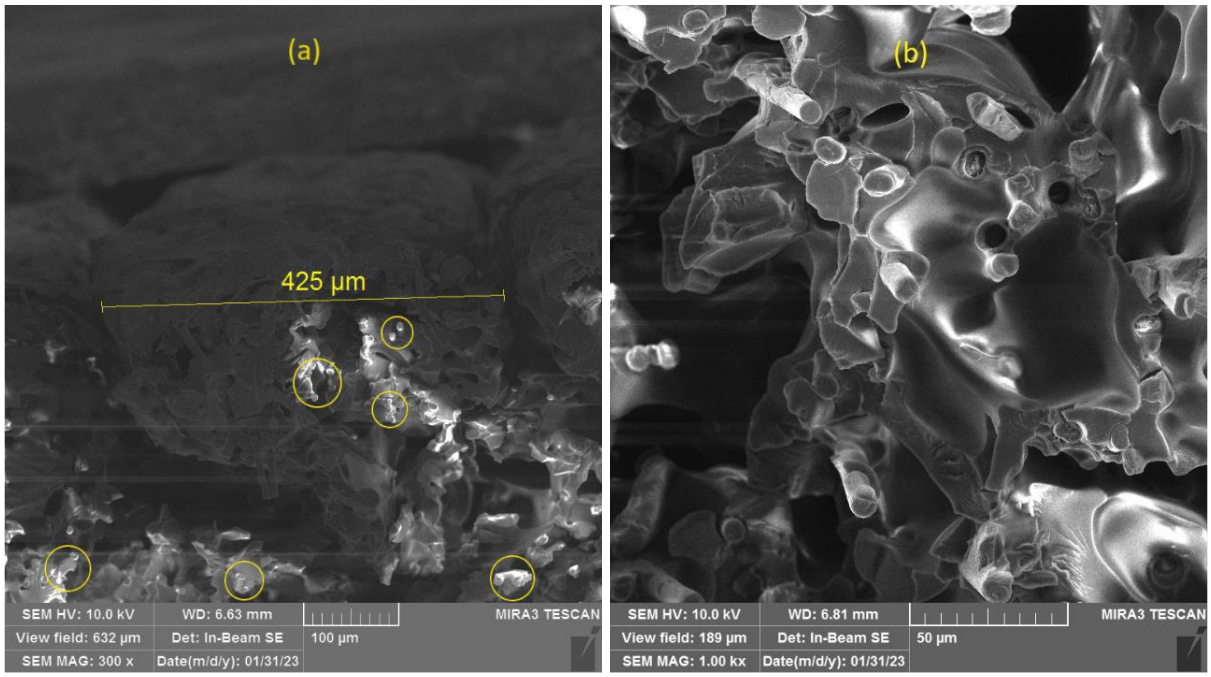

Figure 4.9 *SEM images of fracture surface of the specimen printed with 0° raster angle: (a) raster cross-section together with air gap around it – 300 x magnification; (b) closer look at the captured short carbon fibers – 1000 x magnification*

Figure 4.10a shows the fracture surface of the specimen printed with the 90° raster angle, with a distinct boundary between the subsequent layers. This is because the major voids are positioned between the deposited layers in form of captured air, as anticipated. The highlighted measures of 213 μm and 221 μm in Figure 4.10a comply with the preassigned printing parameter of a layer thickness of 0.2 mm. In Figure 4.10b, the final orientation of carbon fibers is clearly visible. The fibers are generally aligned with the direction of the deposited beads, as concluded from traces where the fibers were placed before being pulled out during the fracture. This conclusion is further supported by the orientation of fibers that remained on the fracture surface of the observed specimen, which can be seen in yellow circles in Figure 4.10b. The poor tensile properties of the 90° raster angle specimens could be attributed to the carbon fibers' alignment, which is in this case perpendicular to the direction of load application, and the weak bonding between two adjacent layers and the presence of voids.

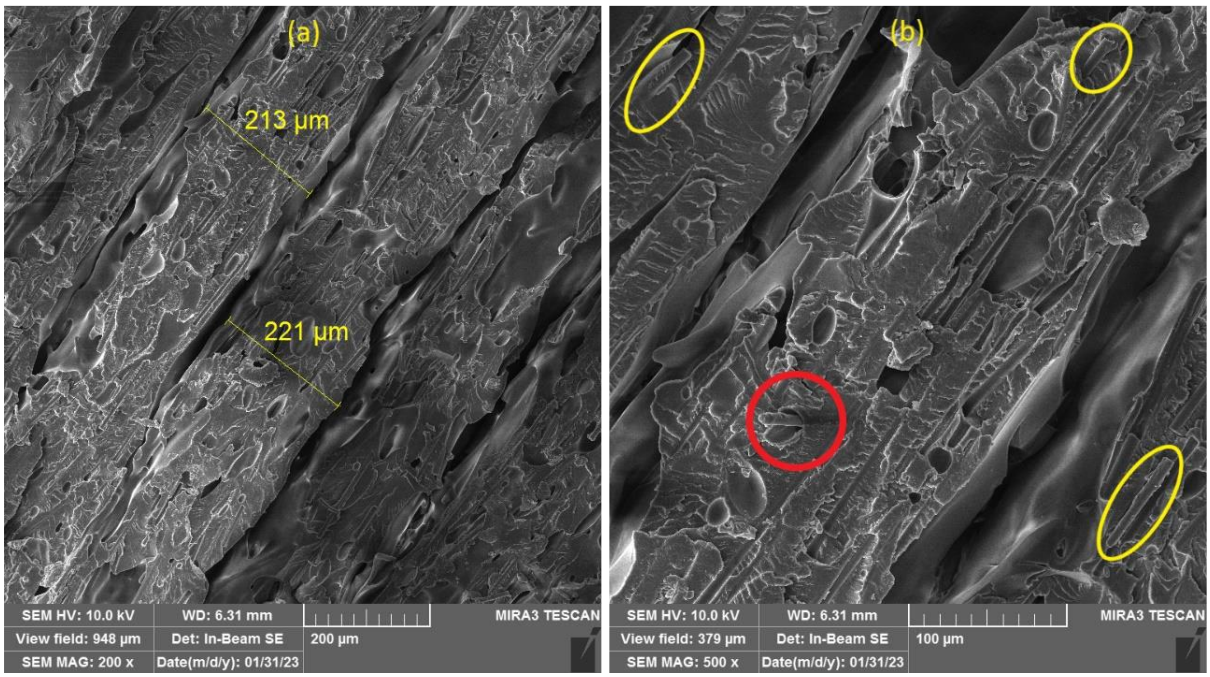

Figure 4.10 *SEM images of fracture surface of the specimen printed with 90° raster angle: (a) layers clearly visible with border between them in form of captured air – 200 x magnification; (b) closer look at the orientation of captured short carbon fibers – 500 x magnification*

It was noticed that a particular number of carbon fibers are not aligned to the printing direction after analysing the recorded SEM images. The filament manufacturing process itself likely resulted in these fibers failing to bond adequately with the polymer matrix. The red circle in Figure 4.10b highlights one of these fibers. Despite that, it is noteworthy that there is actually few such fibers when contrasted to those which are properly "wetted" and adhere to the printing direction. A representative of interface bonding between fiber and polymer is shown in Fig. 4.11a, with measured diameter of the fiber highlighted (9 μm). Figure 4.11b shows a closer view of the fiber with poor bonding that was circled in red in Figure 4.10b.

Despite setting the overlapping to 25% in order to reduce the air gap, SEM images revealed that the raster geometry inherently created noticeable pockets of air that were captured between rasters. According to the SEM images, it is evident that there are also voids within the polymer phase and at the interface between the short carbon fibers and the PET-G polymer. In addition to lowering the effective elastic moduli due to a decrease in the physical cross-sectional area, the existence of these voids may result in high stress concentration factors, which lower the final part's strength properties.

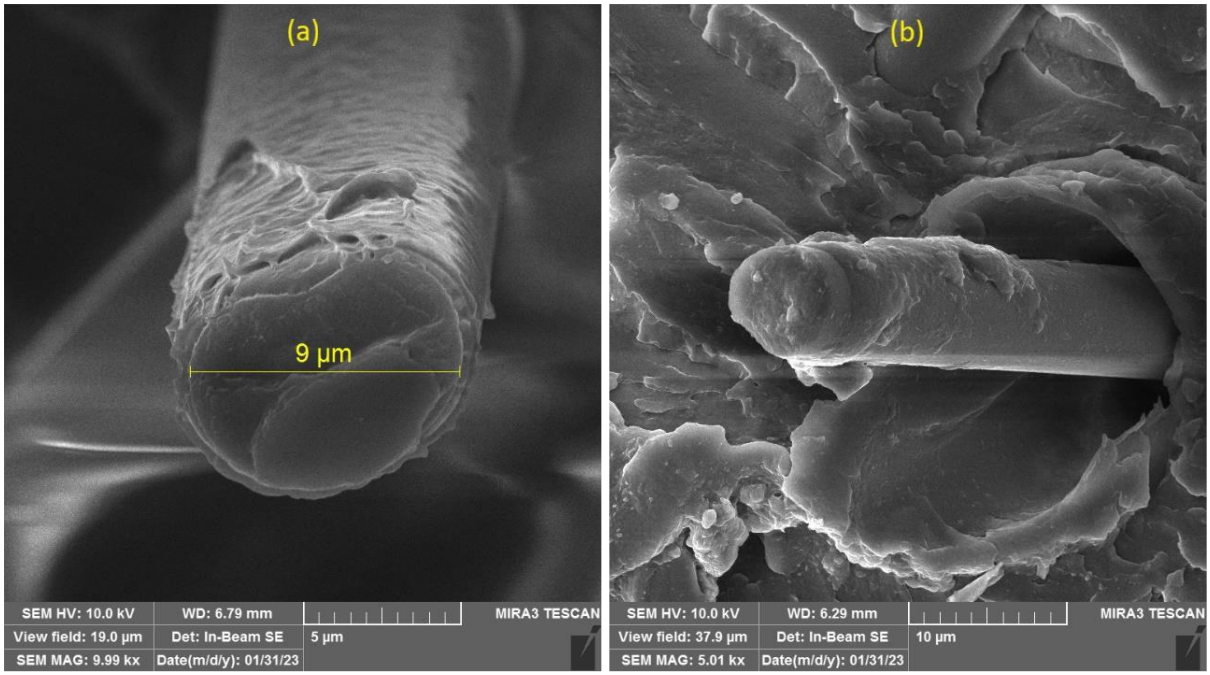

Figure 4.11 *SEM images of (a) an example of good interface bonding between fiber and polymer, with measured diameter of the fiber highlighted – 10000 x magnification and (b) an example of poor bonding – 5000 x magnification*

Results showing a relatively low value (in terms of what was expected) of ultimate tensile strength (52.2 MPa) for samples printed with the 0° raster angle compared to neat PET-G (maximum 46.1 MPa [8]) may be due to the large number of inhomogeneities in the printed material, even though scanning electron microscopy (SEM) images showed that short carbon fibers mainly align with the printing direction and therefore reinforce that particular direction.

4.3 Shear testing and obtained results

In-plane shear properties of SCF-reinforced PET-G specimen (see Figure 4.2) are determined according to a standardised procedure. Three-rail shear test procedure was applied. In this procedure, the test fixture consists of three pairs of parallel rails usually bolted to the test specimen by through bolts (see Figure 4.12). The two outside pairs of rails are joint to the base of fixture which is placed on the universal testing machine (see Figure 4.13). The third pair (center rails) is guided through a slot in the top of the base fixture. A load is introduced onto the center rails and produces a shear load in the specimen. The load may be introduced as either tension or compression, but compression loading is more usual because it does not require attaching the base fixture to the test machine, as presented by the setup in Figure 4.13 which was used for conducting the shear test.

Figure 4.12 *Specimen for shear testing inserted into Three-Rail Shear fixture*

Figure 4.13 *Three-Rail Shear fixture with specimen inserted positioned within the Universal Testing Machine*

Since load-strain data is required, the specimens were instrumented with strain gauges. Load was recorded through the universal testing machine load-sensing device, while strain was measured by strain gauges bonded to the specimen at the pre-assigned locations at the center of the gauge section (in-between the holes for bolts). Linear strain gauges bonded to the specimen at the 45° direction were used to capture extensional strains in that direction. Then, these strain data were used to calculate the corresponding shear strains. After load and strain data are gathered, the required shear stress – shear strain diagram was formulated (see Figure 4.14).

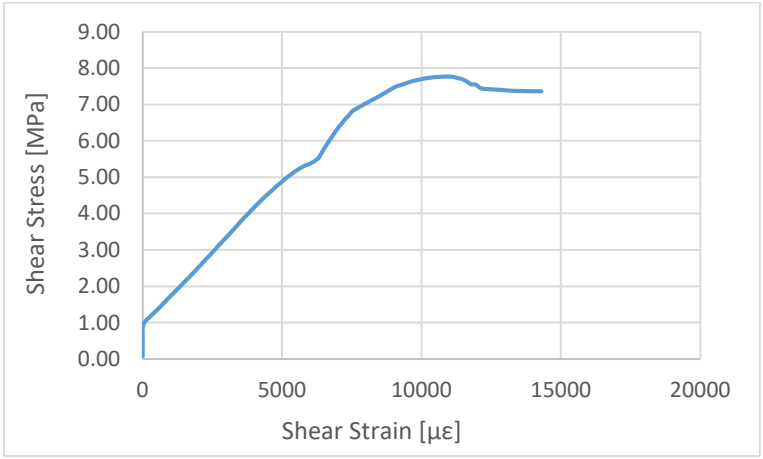

Figure 4.14 *An example of shear stress – shear strain curve obtained for the tested material*

4.4 Applied methodology for obtaining the elastic constants

Methodology applied for obtaining the values for modulus of elasticity, Poisson's ratio, coefficient of mutual influence of the second kind as well as the ultimate tensile strength is presented throughout this Chapter. Values obtained for the aforementioned quantities are summarized for specimens printed with different raster angle patterns ranging from 0° to 90°. These values served afterwards to formulate functional relations presented in Chapter 5.

4.4.1 Modulus of elasticity evaluation

As mentioned earlier in Chapter 4.1, tensile properties of the tested specimens were determined according to the ASTM D638-03 standard [35], under defined conditions of pretreatment, temperature and testing machine speed. Dividing the force data recorded on the tensile testing machine by the pre-measured original cross-sectional area in the gage length segment of the specimen led to gathering the stress data. These data together with the stain data obtained by DIC served for drawing the stress-strain diagrams. As shown in Fig. 4.15, the tangents to the linear-elastic sections of the stress-strain curves were constructed, and the corresponding slopes, which represent the moduli of elasticity, were evaluated. Since there were initial regions on the raw stress-strain curves that does not represent a property of the material (an artifact caused by a takeup of slack and alignment or seating of the specimen), this artifacts were compensated for to give the corrected zero point on the strain axis (so called toe compensation) and diagrams previously shown in Figure 4.5 were obtained.

Table 4.2 displays the mean and standard deviation values of the modulus of elasticity obtained for different raster angle specimen series. All of the measurements have small standard deviations, which indicates good repeatability in the experimental data.

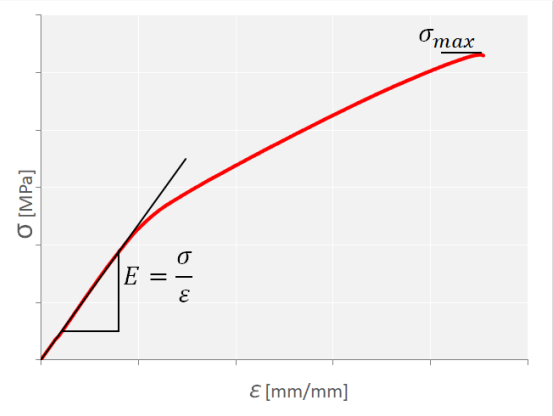

Figure 4.15 *The modulus of elasticity calculation by graphical method (slope of the curve)*

Table 4.2 *Summary of values for modulus of elasticity acquired for different raster angles*

Raster angle [°]	E [MPa]	
	Average	St. Dev.
0	4752	106
15	3709	112
30	2664	64
45	2089	61
60	1573	15
75	1393	33
90	1569	26

4.4.2 Shear modulus evaluation

Fist, the shear stress is calculated based on the load data recorded on the universal testing machine. For the three-rail shear procedure, the shear stress is calculated as follows:

$$\tau = P/2A \ ,$$

where P is load applied to the specimen and A is the cross-sectional area at test section calculated as the product of the average length and average thickness. The normal strain data at 45° (ε_{45}) is determined from strain gauges' readings and the required shear strain is then calculated as follows:

$$\gamma = 2\varepsilon_{45} \ ,$$

by using equations (2.32) and (2.33). Then, the diagram shown in Figure 4.14 is obtained, relating the shear stress to the shear strain.

Now, the shear modulus can be calculated as the ratio of difference in applied shear stress between the two strain points within the linear elastic region and difference between the two shear strains at the corresponding points (see Figure 4.16):

$$G = \Delta\tau/\Delta\gamma$$

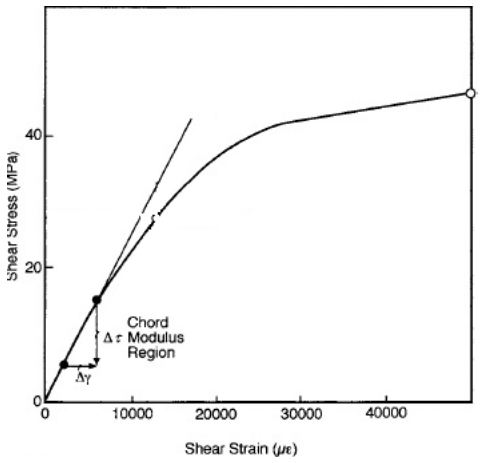

Figure 4.16 *Graphical method for calculating shear modulus (slope of the curve) [36]*

The shear modulus values for the tested specimens were determined in the above described way and are presented in Figure 4.17. The average value of those (753 MPa) is utilised further on throughout the thesis – for establishing correlations between the theoretical (equations (2.77), (2.78) and (2.80)) and experimentally obtained tensile elastic constants in relation to the raster angle.

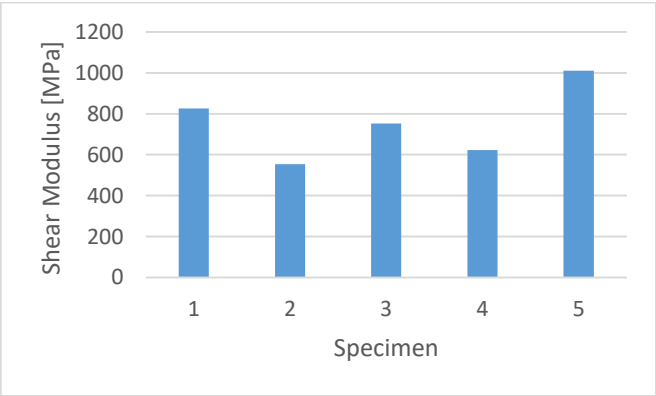

Figure 4.17 *Values obtained for shear modulus*

4.4.3 Poisson ratio evaluation

Following the definition of the Poisson's ratio given in Chapter 2 by the equation (2.54), values for different raster angles were obtained using the data on normal strains given in Table 4.1. Calculated values for the Poisson's ratio are presented in Table 4.3. At first glance, it is noticeable that values obtained for different raster angles differ quite a lot which indicates the anisotropic behaviour of the studied SCF-reinforced PET-G polymer.

Table 4.3 *Summary of values obtained for the Poisson's ratio for different raster angles*

Raster angle [°]	ν [-]
0	0.3765
30	0.3244
45	0.3475
60	0.0810
90	0.0648

4.4.4 Coefficient of mutual influence evaluation

As earlier defined within the Chapter 2, the coefficient of the mutual influence of the second kind represents the effect of anisotropy in the specimen plane (x–y plane) in terms of occurrence of shear strain in the x–y plane (γ_{xy}) due to the action of normal stress e.g. σ_x, while at the same time the following applies: $\sigma_y = \tau_{xy} = 0$. In a similar way the Poisson's ratio values were calculated, values for the coefficient of the mutual influence of the second kind were calculated following the equation (2.57) and using the corresponding normal and shear strain data given in Table 4.1. Calculated values for the coefficient of the mutual influence of the second kind are presented in Table 4.4. Again, it can be noticed that values obtained for different raster angles are different and highlight the presence of the anisotropy in the studied SCF-reinforced PET-G polymer.

Table 4.4 *Summary of values obtained for the Coefficient of the mutual influence of the second kind for different raster angles*

Raster angle [°]	$n_{xy,x}$ [-]
0	0.04503
30	0.86229
45	0.47892
60	0.35006
90	-0.03612

4.5 Strength properties evaluation

Values for the ultimate tensile strengths are directly calculated from the load data recorded by the tensile testing machine as maximum stresses withstood throughout the testing. Namely, tensile strength was obtained by dividing the maximum recorded load (force) by the average original cross-sectional area in the gage length segment of the specimen in square metres. Graphical representation of the ultimate tensile strength (σ_{max}) can be seen in Figure 4.15.

The average and standard deviation values for the ultimate tensile strength are listed in Table 4.5. Similar to the values obtained for modulus of elasticity, standard deviations for strength values are also small which again indicates good repeatability in the experimental data.

Table 4.5 *Summary of values for ultimate tensile strength acquired for different raster angles*

Raster angle [°]	σ_{max} [MPa]	
	Average	St. Dev.
0	52.2	2.5
15	47.8	0.8
30	37.8	0.4
45	33.1	0.5
60	24.7	0.9
75	19.0	0.6
90	25.4	0.4

5 Establishing functional relations

In this Chapter, there will be established functional relations between the tensile elastic constants on the one hand and the corresponding raster angle on the other, together with variation of the ultimate tensile strength property across different raster angles – all derived for thin-plate parts additively manufactured from PET-G polymer reinforced with short carbon fibers. All of the here-referred tensile quantities are determined for seven different raster angles ranging from 0° to 90° (with an increment of 15°) and obtained results are presented throughout the Chapter 4. Here, the results are brought together in form of dependence of the experimentally evaluated tensile mechanical properties on the applied printing direction (raster angle) and hence the direction of most fiber spreading, in order to check for agreement with relations given in equations (2.77), (2.78) and (2.80) widely known for classical composite plates containing continuous fiber reinforcements [34].

5.1 Functional relations between the tensile elastic constants and the raster angle

As for representative tensile elastic constants, modulus of elasticity, Poisson's coefficient and coefficient of mutual influence are considered. These tensile elastic constants were previously defined in Chapter 2 through equations (2.77), (2.78) and (2.80) which can be re-written as:

$$E_x = \frac{1}{\frac{1}{E_1}c^4 + \left[-\frac{2\nu_{12}}{E_1} + \frac{1}{G_{12}}\right]s^2c^2 + \frac{1}{E_2}s^4}, \tag{5.1}$$

$$\nu_{xy} = \frac{\frac{\nu_{12}}{E_1}(s^4 + c^4) - \left[\frac{1}{E_1} + \frac{1}{E_2} - \frac{1}{G_{12}}\right]s^2c^2}{\frac{1}{E_1}c^4 + \left[-\frac{2\nu_{12}}{E_1} + \frac{1}{G_{12}}\right]s^2c^2 + \frac{1}{E_2}s^4}, \tag{5.2}$$

$$n_{xy,x} = -\frac{\left[\frac{2}{E_1} + \frac{2\nu_{12}}{E_1} - \frac{1}{G_{12}}\right]sc^3 + \left[\frac{2}{E_2} + \frac{2\nu_{12}}{E_1} - \frac{1}{G_{12}}\right]s^3c}{\frac{1}{E_1}c^4 + \left[-\frac{2\nu_{12}}{E_1} + \frac{1}{G_{12}}\right]s^2c^2 + \frac{1}{E_2}s^4}, \tag{5.3}$$

where $c = \cos(\theta), s = \sin(\theta)$ while angle θ is the angle related to the direction of reinforcement. As confirmed by SEM images of fracture surfaces, presented in Chapter 4.2.3, raster angle directly corresponds to direction of short carbon fiber reinforcement of PET-G polymer.

As shown by equations (5.1), (5.2) and (5.3), to plot the presented theoretically obtained curves for E_x, ν_{xy} and $n_{xy,x}$ values for E_1, E_2, ν_{12}, G_{12} are needed as inputs. Since raster angle directly corresponds to direction of short carbon fiber reinforcement of PET-G polymer, based on data from Table 3, Table 4 and Figure 17, average values of these inputs appear to be:

$$E_1 = 4752\ MPa, E_2 = 1569\ MPa, \nu_{12} = 0.3765, G_{12} = 753\ MPa \tag{5.4}$$

5.1.1 Modulus of elasticity E_x

The values evaluated for the modulus of elasticity based on tensile testing conducted on the universal testing machine outlined in Chapter 4.4.1 are considered first. By substituting equation (5.4) into equation (5.1) ″theoretical″ expression for E_x is obtained. To compare the obtained values with the ″theoretical″ expression for E_x given through equation (5.1), Matlab® code was formulated. In order to check the matching of experimentally obtained data with theoretical approach, values for the modulus of elasticity listed in Table 4.2. together with their standard deviations are plotted against the theoretical curve for E_x as presented in Figure 5.1.

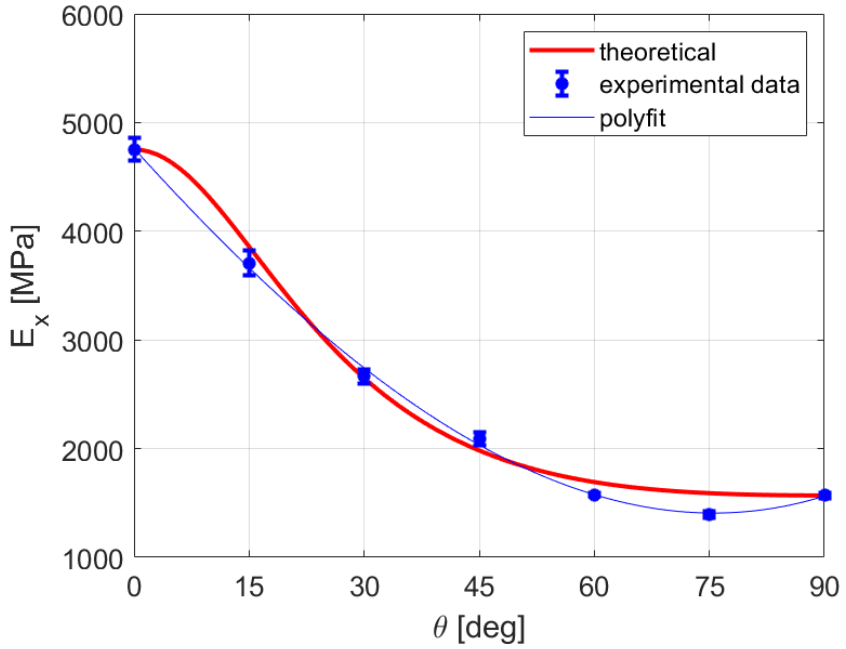

Figure 5.1 *Modulus of Elasticity in relation to raster angle θ*

Looking at the estimated values (red line) calculated by the ″theoretical″ expression for modulus of elasticity - E_x, together with experimentally obtained values (blue dots), there can be seen a high level of matching between these values (differences are less than 10%). This is true for the whole raster angle range.

5.1.2 Poisson's coefficient ν_{xy}

As mentioned in Chapter 4.4.3, calculated values for normal strains (ε_x, ε_y) obtained from DIC results served for determination of values for the Poisson's coefficient ν_{xy} - see Table 2. By definition, in case when loading is applied in the direction aligned with axis x, Poisson's ratio ν_{xy} is the following quotient:

$$\nu_{xy} = -\varepsilon_y/\varepsilon_x \,. \tag{5.5}$$

Thus, experimentally obtained values for Poisson's coefficient ν_{xy} were presented in Table 4.3. As shown in Figure 5.2 these values are plotted versus different values of raster angles observed. Standard deviations of the obtained values (from Table 4.3) are also incorporated in the plot. Similar to the aforementioned Matlab® code used for the modulus of elasticity variation with the reinforcement direction, here the ″theoretical″ expression for the

Poisson coefficient ν_{xy} was employed through equation (5.2), again utilising values for E_1, E_2, ν_{12}, G_{12} as inputs – see equation (5.4). The applicability of the ″theoretical″ expression given through equation (5.2) to determine the Poisson's coefficient ν_{xy} for the additively manufactured PET-G polymeric material reinforced with SCF is considered based on contrast between the theoretical and the experimental data as shown in Figure 5.2.

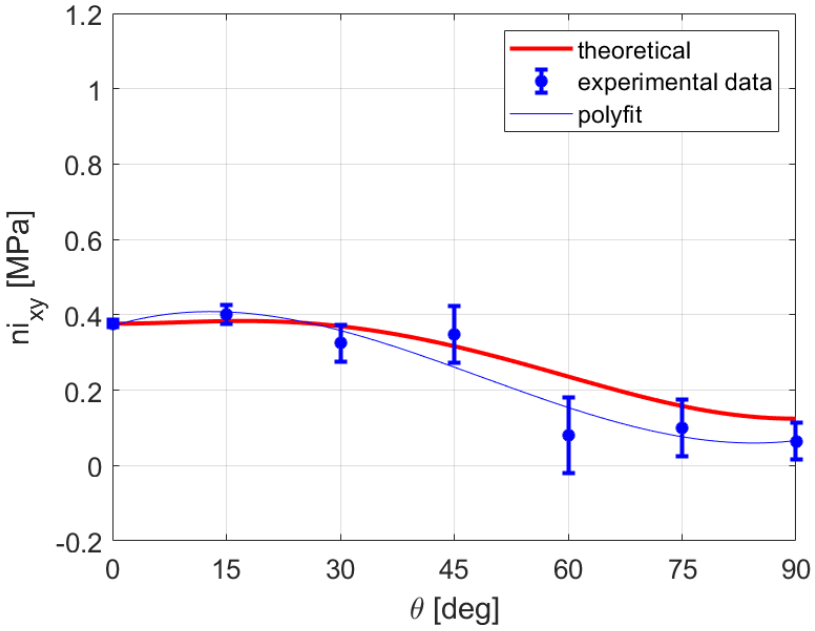

Figure 5.2 *Poisson's coefficient in relation to raster angle θ*

Comparing the estimated values calculated by the ″theoretical″ expression for Poisson's coefficient - ν_{xy} (red line) with experimentally obtained values (blue dots) presented in Figure 5.2, mismatching of the values can be noticed, particularly in the 45°- 75° raster angle range. This is in contrast to results presented in Figure 5.1 for modulus of elasticity, where experimental values were aligned to the ″theoretical″ ones for the whole raster angle range.

5.1.3 Coefficient of mutual influence $n_{xy,x}$

Experimentally obtained values for normal strain ε_x and in-plane shear strain γ_{xy} obtained from DIC results, as presented in Chapter 4.4.4 - Table 4.1, served for determination of values for the coefficient of mutual influence $n_{xy,x}$. By definition, in case when loading is applied in the direction aligned with axis x, coefficient of mutual influence $n_{xy,x}$ is the following quotient:

$$n_{xy,x} = -\gamma_{xy}/\varepsilon_x \,. \tag{5.6}$$

Thus, experimentally obtained values for coefficient of mutual influence $n_{xy,x}$ with their standard deviations were presented in Table 4.4. Here, the ″theoretical″ expression for the coefficient of mutual influence $n_{xy,x}$was employed through equation (5.3), again utilising values for E_1, E_2, ν_{12}, G_{12} as inputs – see equation (5.4). The ″theoretical″ variation of the coefficient of mutual influence with change in the reinforcement orientation is shown in Figure 5.3. Again, corresponding Matlab® code was formulated to plot experimentally obtained and theoretically determined values for the coefficient of mutual influence (Figure 5.3).

The applicability of the ″theoretical″ expression given through equation (5.3) to determine coefficient of mutual influence $n_{xy,x}$ for the additively manufactured PET-G polymeric material reinforced with SCF is considered based on contrast between the theoretical and the experimental data as shown in Figure 5.3.

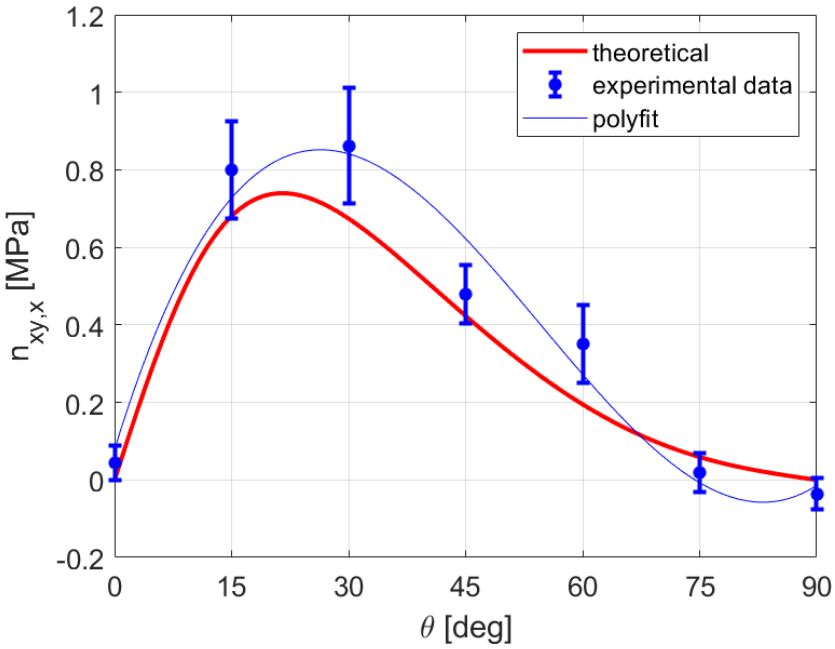

Figure 5.3 *Coefficient of mutual influence $n_{xy,x}$ in relation to raster angle θ*

Similar to results obtained for the Poisson's ratio, comparison of the estimated values calculated by the ″theoretical″ expression for the coefficient of mutual influence of the second kind - $n_{xy,x}$ (red line) with the experimentally obtained values (blue dots) presented in Figure 5.3 does not show adequate matching, particularly in 15°- 60° raster angle range. However, the experimental values are converging to the theoretical curve, but are not closely aligned to the curve, as the case was with the modulus of elasticity values in Figure 5.1

5.2 Functional relations between the tensile strength and the raster angle

In the case of observing the maximum stress which additively manufactured SCF-reinforced PET-G specimens withstood throughout the tensile testing, it is helpful to tentatively understand or even try to predict failure in terms of final fracture as a phenomenon proved to be directly dependant on the raster angle applied while printing. Accordingly, experimentally obtained results for the ultimate tensile strength (see Chapter 4.5) showed various strength characteristics for different raster angles and thus SCF reinforcement orientations. This fact ultimately directly confirmed the anisotropic nature of the studied additively manufactured SCF-reinforced PET-G specimens. These results are presented graphically in Figure 5.4 combined with proposed functional relation between the ultimate tensile strength on the one hand and the raster angle on the other one. Third order polynomial fitting of the experimentally obtained values was utilised to create the continuous UTS-raster angle relation shown in Figure 5.4.

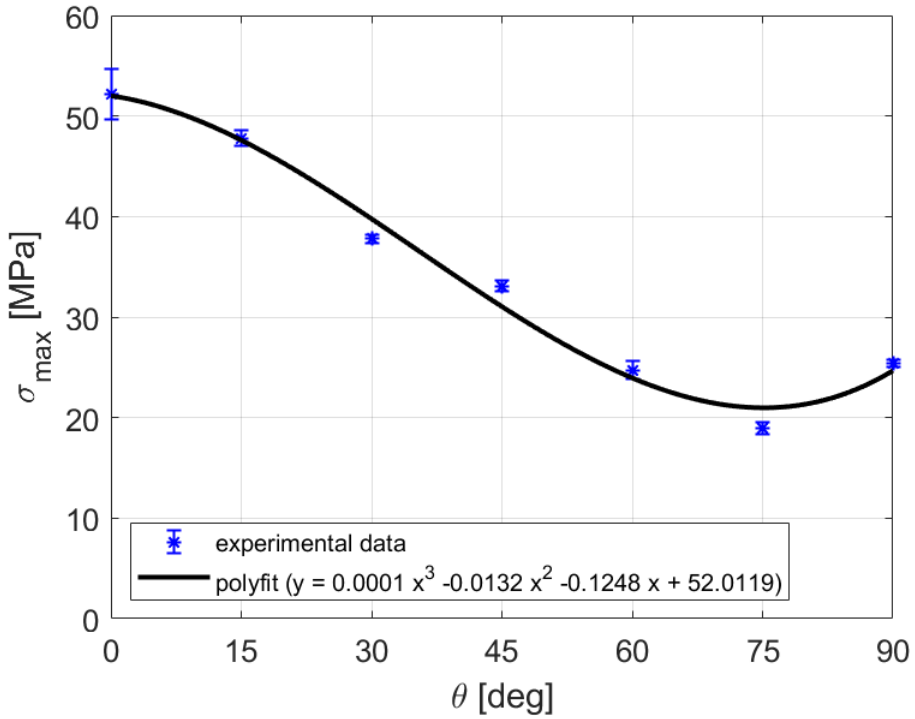

Figure 5.4 *Proposed functional relation between the ultimate tensile strength and the raster angle which fits the experimentally obtained values*

Due to anisotropic nature of the studied parts the use of classical failure criteria used in case of isotropic materials (e.g. von-Mises, Tresca etc.) is not applicable. Therefore, further investigation regarding prediction of failure for additively manufactured SCF-reinforced PET-G polymer material is needed.

6 Conclusion and future research

In additive manufacturing (AM), raster angle is recognized as one of the key printing parameters which strongly influences the strength and stiffness of the final part. In this thesis the effect of raster angle on tensile properties of thin plate specimens made from carbon reinforced PET-G material was studied. The major objectives were to establish and analyse a functional relation between the corresponding raster angle and:

- obtained values of tensile strength and stiffness of plate specimens made from carbon reinforced PET-G material;

- the tensile elastic constants that define the anisotropic behaviour of plate specimens made from carbon reinforced PET-G material, primarily modulus of elasticity - E_x, Poisson's coefficient - ν_{xy} and coefficient of mutual influence of the second kind - $n_{xy,x}$.

Aforementioned functional relations were compared with theoretical results given by the Classical Lamination Theory (CLT).

6.1 Conclusions

As a result of the research within this thesis, it is confirmed that raster angle strongly influences the strength and stiffness of final additively manufactured thin plate parts made from short carbon reinforced PET-G material.

The relatively high average value of ultimate tensile strength - 52.2 MPa was obtained for specimens printed with the raster angle of 0°, compared to the value obtained for specimens printed with the raster angle of 90° - 25.4 MPa. The minimum average value of ultimate tensile strength was obtained for specimens printed with the raster angle of 75° - 19.0 MPa which indicates decrease of 63.6% (compared to value for the 0° raster angle). Similarly, the maximum obtained average value of modulus of elasticity - 4752 MPa was obtained for specimens printed with the raster angle of 0° compared to the value of 1569 MPa, obtained for specimens printed with the raster angle of 90°. Again, the minimum average value of modulus of elasticity was obtained for specimens printed with the raster angle of 75° - 1393 MPa, which indicates decrease of 70.7% (compared to value for the 0° raster angle).

SEM images of fracture surfaces of the specimens printed with the 0° raster angle revealed dominant alignment of short carbon fibers with the printing direction applied, but also moderate to high level of inhomogeneity and voids. Considerable volume fraction of captured air (air gaps) with noticeable amount of porosity in polymer phase are probably major factors which resulted in relatively low improvement of tensile strength obtained for carbon reinforced samples made with the 0° printing direction, when compared to neat polymer samples. In the similar manner, voids together with weak bonding between two adjacent rasters undoubtedly contributed to poor tensile properties of carbon reinforced samples made with the raster angle of 90°.

Comparison of the estimated values calculated by the ″theoretical″ expression for modulus of elasticity - E_x given through equation (5.1), with experimentally obtained values listed in Table 4.2 presented in Figure 5.1, showed almost perfect matching (mismatching was less than 10% for whole raster angle range). In case of Poisson's coefficient - ν_{xy} and

coefficient of mutual influence of the second kind - $n_{xy,x}$ mismatching was higher than 10% for whole raster angle range. Thus, comparison of the estimated values calculated by the ″theoretical″ expression for Poisson's coefficient - ν_{xy} given through equation (5.2), with experimentally obtained values listed in Table 4.3, presented in Figure 5.2, showed significant mismatching particularly in 45°- 75° raster angle range. Similarly, comparison of the estimated values calculated by the ″theoretical″ expression for coefficient of mutual influence of the second kind - $n_{xy,x}$ given through equation (5.3), with experimentally obtained values listed in Table 4.4, presented in Figure 5.3, showed significant mismatching particularly in 15°- 60° raster angle range.

On the other hand, experimentally obtained results for the ultimate tensile strength, shown in Figure 5.4, showed similar behaviour found in laminated composite plates reinforced with continuous carbon fibers. This fact ultimately directly confirmed the anisotropic nature of the studied additively manufactured SCF-reinforced PET-G specimens. These results are presented graphically in Figure 5.4 combined with proposed functional relation between the ultimate tensile strength on the one hand and the raster angle on the other one.

6.2 Future research

It is expected the thesis will contribute to the definition of future constitutive model that will enable the application of numerical structural analysis on thin plate-like parts made from observed material composition and produced by additive manufacturing. Accordingly, it is also expected that the dissertation will contribute to a better understanding and further enhancements in possible applications of this type of composite materials for quick and efficient production of parts intended for moderate loadings.

Experimentally obtained strengths (e.g. presented in Table 4.5) are usually obtained as a result of conducted procedures defined by standard definitions which involve that these experiments must be carried out at standard room temperature. Possible future research might involve low temperature conditions for experiments used for obtaining quoted strengths. Therefore, it might be interesting to analyze how ultimate strength values, experimentally obtained at extremely low or extremely high temperatures, contribute to potential reduction of strength of short carbon fiber reinforced AM structures.

Due to anisotropic nature of the studied parts the use of classical failure criteria used in case of isotropic materials (e.g. von-Mises, Tresca etc.) is not applicable. Therefore, further investigation regarding prediction of failure for additively manufactured SCF-reinforced PET-G polymer material is needed.

7 Literature

[1] I.M. Daniel, O. lshai, Engineering Mechanics of Composite Materials, Oxford University Press (2006)

[2] J. Barbero, Introduction to Composite Materials Design, CRC Press (2017)

[3] Jean-Marie Berthelot, Mechanics of Composite Materials and Structures (2015)

[4] Hyer, M. W., Stress analysis of fiber-reinforced composite materials, DEStech Publications, Inc (2009)

[5] R. Aleksić, I. Živković, P. Uskoković, Kompozitni materijali, Tehnološko metalurški fakultet Univerziteta u Beogradu (2015)

[6] B. Redwood, F. Schöffer, B. Garret, The 3D Printing Handbook, Technologies, design and applications, 3D Hubs (2017)

[7] Z. Quan, A. Wu, M. Keefe, X. Qin, J. Yu, J. Suhr, J-H. Byun, B-S. Kim, T-W. Chou, Additive manufacturing of multi-directional preforms for composites: Opportunities and challenges, Materials Today, 18(9) (2015) 503-512

[8] S.M.F. Kabir, K. Mathur, A.F.M. Seyam, A critical review on 3D printed continuous fiber - reinforced composites: History, mechanism, materials and properties, Composite Structures 232 (2020) 111476

[9] N. van de Werken, H. Tekinalp, P. Khanbolouki, S. Ozcan, A. Williams, M. Tehrani, Additively manufactured carbon fiber -reinforced composites: State of the art and perspective, Additive Manufacturing 31 (2020) 100962

[10] D. Jiang, D. E. Smith, Anisotropic mechanical properties of oriented carbon fiber filled polymer composites produced with fused filament fabrication, Additive Manufacturing 18 (2017) 84–94

[11] H. L. Tekinalp, V. Kunc, G. M. Velez-Garcia, C. E. Duty, L. J. Love, A. K. Naskar, C. A. Blue, S. Ozcan, Highly oriented carbon fiber–polymer composites via additive manufacturing, Composites Science and Technology 105 (2014) 144–150

[12] M. Ivey, G.W. Melenka, J.P. Carey, C. Ayranci, Characterizing short-fiber-reinforced composites produced using additive manufacturing, Advanced Manufacturing: Polymer & Composites Science 3:3 (2017) 81-91

[13] S. Adil, I. Lazoglu, A review on additive manufacturing of carbon fiberreinforced polymers: Current methods, materials, mechanical properties, applications and challenges, Journal of Applied Polymer Science (2023), 140(7)

[14] A. Bisoi, M. Tüfekci, V. Öztekin, E.D. Goy, L. Salles, Experimental Investigation of Mechanical Properties of Additively Manufactured Fibre-Reinforced Composite Structures for Robotic Applications, Applied Composite Materials 31 (2024) 421–446

[15] J.M. Chacón, M.A. Caminero, E. García-Plaza, P.J. Núñez, Additive manufacturing of PLA structures using fused deposition modelling: Effect of process parameters on mechanical properties and their optimal selection, Materials and Design 124 (2017) 143–157

[16] N. Zohdi, R.C. Yang, Material Anisotropy in Additively Manufactured Polymers and Composites: A Review, Polymers 13 (2021) 3368

[17] M. Popović, M. Pjević, A. Milovanović, G. Mladenović, M. Milošević, Printing parameter optimization of PLA material concerning geometrical accuracy and tensile properties relative to FDM process productivity, Journal of Mechanical Science and Technology, 37 (2023) 697-706

[18] M. Somireddy, C.V. Singh, A. Czekanski, Mechanical behaviour of 3D printed composite parts with short carbon fiber reinforcements, Engineering Failure Analysis (2019)

[19] A.Y. Al-Maharma, S.P. Patil, B. Markert, Effects of porosity on the mechanical properties of additively manufactured components: a critical review, Materials Research Express 7 (2020) 122001

[20] J. Brackett, D. Cauthen, J. Condon, T. Smith, N. Gallego, V. Kunc, C. Duty, Characterizing the influence of print parameters on porosity and resulting density, Conference Paper - Conference: Solid Freeform Fabrication 2019: Proceedings of the 30th Annual International Solid Freeform Fabrication Symposium – An Additive Manufacturing Conference at: Austin, TX

[21] A. Maguire, N. Pottackal., M.A.S.R. Saadi, M.M. Rahman, P. Ajayan, Additive manufacturing of polymer-based structures by extrusion technologies, Review article, Oxford Open Materials Science, 1(1) (2021) itaa004, doi: 10.1093/oxfmat/itaa004

[22] J.R. Dizon, A.H. Espera Jr., Q. Chen, R. C. Advincula, Mechanical characterization of 3D-printed polymers, Additive Manufacturing 20 (2018) 44-67

[23] E. Cuan-Urquizo, E. Barocio, V. Tejada-Ortigoza, R. B. Pipes, C. A. Rodriguez, A. Roman-Flores, Characterization of the Mechanical Properties of FFF Structures and Materials: A Review on the Experimental, Computational and Theoretical Approaches, Materials (2019)

[24] B. Almeshari, H. Junaedi, M. Baig, A. Almajid, Development of 3D printing short carbon fiber reinforced polypropylene composite filaments, Journal of Materials Research and Technology 24 (2023) 16-26

[25] A. F. Calles, D. Carou, R. T. Luiz Ferreira, Experimental Investigation on the Effect of Carbon Fiber Reinforcements in the Mechanical Resistance of 3D Printed Specimens, Applied Composite Materials (2021)

[26] E. Lobov, A. Dobrydneva, I. Vindokurov, M. Tashkinov, Effect of Short Carbon Fiber Reinforcement on Mechanical Properties of 3D-Printed Acrylonitrile Butadiene Styrene, Polymers 15 (2023)

[27] K.M. Pradeep, P. Senthil, Prediction of in-plane stiffness of multi-material 3D printed laminate parts fabricated by FDM process using CLT and its mechanical behaviour under tensile load, Materials Today Communications 23 (2020) 100955

[28] C. Casavola, A. Cazzato, V. Moramarco, C. Pappalettere, Orthotropic mechanical properties of fused deposition modelling parts described by classical laminate theory, Materials and Design 90 (2016) 453–458

[29] S. S. Ganesh Iyer, O. Keles, Effect of raster angle on mechanical properties of 3D printed short carbon fiber reinforced acrylonitrile butadiene styrene, Composites Communications 32 (2022) 101163

[30] M. Spoerk, C. Savandaiah, F. Arbeiter, G. Traxler, L. Cardon, C. Holzer, J. Sapkota, Anisotropic properties of oriented short carbon fibre filled polypropylene parts fabricated by extrusion-based additive manufacturing, Composites Part A 113 (2018) 95-104

[31] M. Domingo-Espin, S. Borros, N. Agullo, A.A. Garcia-Granada, G. Reyes, Influence of building parameters on the dynamic mechanical properties of polycarbonate fused deposition modeling parts, 3D Printing and Additive Manufacturing, 1 (2014) 70–77

[32] A. Elayeb, M. Janković, S. Dikić, D. Bekrić, I. Balać, Influence of Raster Angle on Tensile Properties of FDM Additively Manufactured Plates made from Carbon Reinforced PET-G Material, Science of Sintering, 55 (2023) 259-268

[33] B.G. Compton, J.A. Lewis, 3D-Printing of Lightweight Cellular Composites, Advanced Materials (2014)

[34] R. M. Jones, Mechanics of Composite Materials, Second Edition, Taylor & Francis Ltd. (1999)

[35] ASTM D638-03 – Standard Test Method for Tensile Properties of Plastics

[36] ASTM D4255-01 – Standard Test Method for In-Plane Shear Properties of Polymer Matrix Composite Materials by the Rail Shear Method